



HAL
open science

Electron Storage System Based on a Two-Way Inversion of Redox Potentials

Alexis Gosset, Liam Wilbraham, Štěpánka Nováková Lachmanová, Romana Sokolová, Grégory Dupeyre, Fabien Tuyèras, Philippe Ochsenbein, Christian Perruchot, Henri-Pierre Jacquot de Rouville, Hyacinthe Randriamahazaka, et al.

► **To cite this version:**

Alexis Gosset, Liam Wilbraham, Štěpánka Nováková Lachmanová, Romana Sokolová, Grégory Dupeyre, et al.. Electron Storage System Based on a Two-Way Inversion of Redox Potentials. *Journal of the American Chemical Society*, 2020, 142 (11), pp.5162-5176. 10.1021/jacs.9b12762 . hal-03084130

HAL Id: hal-03084130

<https://hal.science/hal-03084130v1>

Submitted on 20 Dec 2020

HAL is a multi-disciplinary open access archive for the deposit and dissemination of scientific research documents, whether they are published or not. The documents may come from teaching and research institutions in France or abroad, or from public or private research centers.

L'archive ouverte pluridisciplinaire **HAL**, est destinée au dépôt et à la diffusion de documents scientifiques de niveau recherche, publiés ou non, émanant des établissements d'enseignement et de recherche français ou étrangers, des laboratoires publics ou privés.

1
2
3
4
5 **Electron Storage System Based on a Two-Way Inversion**
6 **of Redox Potentials**
7
8
9

10 Alexis Gosset,^a Liam Wilbraham,^b Štěpánka Nováková Lachmanová,^c Romana Sokolová,^c
11 Grégory Dupeyre,^a Fabien Tuyèras,^a Philippe Ochsenein,^d Christian Perruchot,^a Henri-
12 Pierre Jacquot de Rouville,^{a,f} Hyacinthe Randriamahazaka,^{*,a} Lubomír Pospíšil,^{*,c,e} Ilaria
13 Ciofini,^{*,b} Magdaléna Hromadová,^{*,c} Philippe P. Lainé^{*,a}
14
15
16
17
18
19
20

21 ^a Université de Paris, ITODYS, CNRS, UMR 7086, 15 rue J-A de Baïf, F-75013 Paris,
22 France
23

24 ^b Chimie ParisTech, PSL University, CNRS, Institute of Chemistry for Life and Health
25 Sciences, Theoretical Chemistry and Modelling, 11 rue Pierre et Marie Curie, 75005 Paris,
26 France
27
28

29 ^c J. Heyrovský Institute of Physical Chemistry of the Czech Academy of Sciences,
30 Dolejškova 3, 182 23 Prague, Czech Republic
31

32 ^d Laboratoire de Cristallographie et Modélisation Moléculaire du Solide, Sanofi LGCR, 371
33 rue du Professeur Blayac, 34184 Montpellier Cedex 04, France
34

35 ^e Institute of Organic Chemistry and Biochemistry of ASCR, v.v.i., Flemingovo n.2, 166 10
36 Prague, Czech Republic
37
38
39

40
41 ^f Present address: Université de Strasbourg, Institut de Chimie de Strasbourg (UMR CNRS
42 7177), Institut Le Bel, 4, rue Blaise Pascal, 67000 Strasbourg-France
43
44
45

46
47
48 E-mail: hyacinthe.randria@univ-paris-diderot.fr;
49 Ilaria.ciofini@chimie-paristech.fr; magdalena.hromadova@jh-
50 inst.cas.cz; lubomir.pospisil@jh-inst.cas.cz;
51 philippe.laine@univ-paris-diderot.fr
52
53
54
55
56
57
58
59
60

Abstract.

Molecular-level multielectron handling towards electrical storage, is a worthwhile approach to solar energy harvesting. Here, a strategy which uses chemical bonds as electron reservoirs is introduced to demonstrate the new concept of "structronics" (a neologism derived from "structure" and "electronics"). Through this concept, we establish, synthesize, and thoroughly study two multicomponent "super-electrophores": 1,8-dipyridyliumnaphthalene, **2**, and its *N,N*-bridged cyclophane-like analogue, **3**. Within both of them, a covalent bond can be formed and subsequently broken electrochemically. These super-electrophores are based on two electrophoric (pyridinium) units that are, on purpose, spatially arranged by a naphthalene scaffold. A key characteristic of **2** and **3** is that they possess a LUMO that develops through space as the result of the interaction between the closely-positioned electrophoric units. In the context of electron storage, this "super-LUMO" serves as an empty reservoir, which can be filled by a two-electron reduction, giving rise to an elongated C-C bond or "super-HOMO". Because of its weakened nature, this bond can undergo an electrochemically driven cleavage at a significantly more anodic - yet accessible - potential, thereby restoring the availability of the electron pair (reservoir emptying). In the representative case study of **2**, an inversion of potential in both of the two-electron processes of bond formation and bond-cleavage is demonstrated. Overall, the structronic function is characterized by an electrochemical hysteresis and a chemical reversibility. This structronic super-electrophore can be viewed as the three-dimensional counterpart of benchmark methyl viologen.

1. Introduction

In the context of global warming^{1,2} the sun is now recognized as a relevant alternative to fossil fuels.^{3,4} Multifarious technological and societal changes are deemed to accompany this advent to make possible the desirable change of primary energy source in optimal conditions.^{5,6} As is the case in natural photosynthesis, its artificial counterpart⁷ as well as man-made devices meant to solar energy transduction (e.g. photovoltaics, DSSCs)⁸ largely rely on electrons for their functioning. Likewise, both the handling of multi-electron/hole accumulation and the storage of electricity is performed using chemical energy, whether these processes occur within nature or within artificial setups such as batteries and fuel cells.

Here we tackle the fundamental issue of the extent to which a working principle for the storage of electrons can be established at the molecular level, combining chemical reversibility (represented by cyclability in secondary electric batteries) with the thermodynamic irreversibility of the bond formation and cleavage processes of fuel cells. To do so, we assess the possibility of using electrochemistry, exploiting non-catalyzed processes of formation and cleavage of a single chemical bond. This bond is conceived for its dual ability of being formed upon attaching electrons as the only reagents, that is upon reduction, and to yield electrons upon breaking it that is, upon oxidation (in analogy to the charging and discharging of secondary batteries). We refer to this concept as *structronics* (from "structural" and "electronics"), which is characterized by "using a chemical bond as a *reservoir* for electron storage". As this concept concerns the ability to go back and forth between binary states (chemical reversibility combined with thermodynamic irreversibility), it is closely related to the notion of *electrochemical hysteresis* (see Scheme S1 in SI) and proceeds

1
2
3 according to a two-way inversion of redox potentials. Thereby
4 *storage* is distinguished from the mere process of charges
5 (electrons) *accumulation*,^{4c,d} which rather refers to
6 thermodynamically reversible processes, or alike.^{9,10}
7
8
9

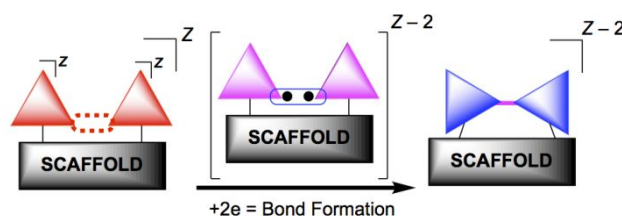
10 Fundamentally, this concept represents a core
11 functionality and, as such, with the exchanged electrons as
12 energy vectors may serve as a means for energy storage.
13 Indeed, in the context of solar energy conversion, given that
14 light absorption is a one-photon process that results in a
15 one-electron charge-separation process,^{4c} at least two of
16 those photons are formally "consumed" per structronic
17 functional species for its charging i.e. C-C bond formation,
18 hence the relevance of using such a bond for photo-
19 electrochemical energy storage (two-photon/two-electron gated
20 reversible Carbon-Carbon bond).¹¹ Last, thanks to hysteretic
21 behavior of the structronic elements, these can serve as a
22 means for the molecular-level storage of information
23 (molecular electronics).¹²
24
25
26
27
28
29
30
31
32
33
34
35

36 **2. Molecular design**

37 For molecular-level charge confinement, the adverse
38 effect to be overcome is the ubiquitous electrostatic
39 repulsion of like charges for both charge *accumulation* and
40 *storage*. Detailed explanation of these two terms in
41 connection with the herein reported molecular design of
42 charge reservoirs, is given in Section S3 of the SI.
43
44
45
46
47

48 The redox-active units of reservoirs are initially
49 defined in their closed-shell native redox state, represented
50 by their initial charge $[z]$. This notation extends to their
51 reactive (i.e. open-shell) radical states, which may be
52 obtained following a one-electron reduction $[z - 1]$ or a one-
53 electron oxidation $[z + 1]$ process. Similarly, species
54 obtained after a two-electron reduction are denoted as $[z -$
55 $2]$. Based on energetics, cationic units are preferred as
56
57
58
59
60

1
2
3 electrophoric components for electrons whereas neutral or
4 anionic units are preferred for holes. In both cases, the
5 design strategy consists of assembling electrophoric
6 subsystems so as to *formally* generate closely lying radicals
7 upon reduction or oxidation, thereby *formally* preparing them
8 for the formation of the reservoir bond (Chart 1). The scope
9 of the present work is restricted to the simplest case of a
10 prototypical covalent assembly based on monocationic
11 electrophoric components ($z = 1+$) that are involved in the
12 reductive formation (and the oxidative cleavage) of a two-
13 electron bond, which functions as a two-electron reservoir.
14
15
16
17
18
19
20
21



22
23
24
25
26
27
28
29 **Chart 1.** Generic representation of the molecular design strategy of the
30 three-dimensional super-electrophore assembly ("structronics" function),
31 which is disconnected from any mechanistic considerations. Electrophoric
32 units (triangles) are pre-organized by the scaffold (spatial layout and
33 strain tuning). The charge of cationic super-electrophore here amounts to
34 $[Z] = [z] + [z] = 2+$ in its native redox state.
35

36
37 At this stage, the question is raised as to whether 2-
38 electron/2-center or 2-electron/ n -center (i.e. "pancake")¹³
39 covalent bonds are the most suitable to function as electron
40 reservoirs. The selection of the former is primarily dictated
41 by the feasibility of a *mechanical* cleavage of the bond on-
42 demand, that is, the a priori possibility of restoring the
43 availability of the electrons (discharging process) using an
44 electro-chemo-mechanical effect or the coupling with a
45 stimulus-responsive molecular actuator. It remains
46 nonetheless that this selection will have to be validated.
47 Above-mentioned critical feature requires that this reservoir
48 bond is conveniently weakened i.e., properly elongated. It
49 follows that the choice of the scaffold responsible for (pre-
50 assembling (and constraining) the electrophoric units is
51
52
53
54
55
56
57
58
59
60

1
2
3 crucial. In addition to setting-up a precise spatial layout
4 of the redox-active components, it ensures the adequate
5 straining, and therefore weakening, of the inter-
6 electrophoric reservoir bond, once formed (Chart 1). Brought
7 together, the electrophoric units and the assembling unit
8 (scaffold) are the basic functional elements that allow the
9 implementation of structronic function, that is, *hysteretic*
10 *electrochemical behavior* for storage, giving rise to the
11 specific covalent architecture referred to as a *super-*
12 *electrophore* (in this context, a *bistable* system). Even
13 though the process of bond formation/cleavage is expected to
14 be chemically reversible, the molecular-level function relies
15 on *thermodynamic irreversibility* that, here, takes the form
16 of bistability, with different electrochemical pathways for
17 bond formation and bond cleavage.

18
19
20 The whole aim of this proof of concept paper is to
21 engineer the inter-component (through-space) orbital overlap
22 to yield a LUMO which functions as a "two-electron trap".
23 Therefore, one must switch the point of reductive reactivity
24 from the individual electrophoric components to the super-
25 electrophoric assembly as a whole.

26
27
28 Based on the above-defined criteria, we consider the
29 pyridinium moiety as electrophoric component (Chart 2). This
30 choice was made firstly because of the intrinsically uneven
31 distribution of atomic contributions to the LUMO over its
32 heteroaromatic ring, characterized by the large involvement
33 of the carbon atom at the γ position ($C(\gamma)$; Chart 2a)¹⁴ and
34 secondly, for its ability to rather easily overcome
35 aromaticity to adopt a post-reduction quinoidal structure.¹⁵
36 Furthermore, pyridinium derivatives are remarkably versatile,
37 especially regarding their redox properties, which can be
38 tuned over a range of potentials of *c.a.* 1.5 V.¹⁶ As the
39 scaffold, we selected the naphthalene platform (with 1,8-
40 connectivity) that has the great asset of being structurally
41
42
43
44
45
46
47
48
49
50
51
52
53
54
55
56
57
58
59
60

flexible enough through skeletal distortion,^{17,18} which is of interest for adjusting the strain on the reservoir bond (whether via cross clamping, front strain or remote (back) strain; Chart 2c).¹⁹

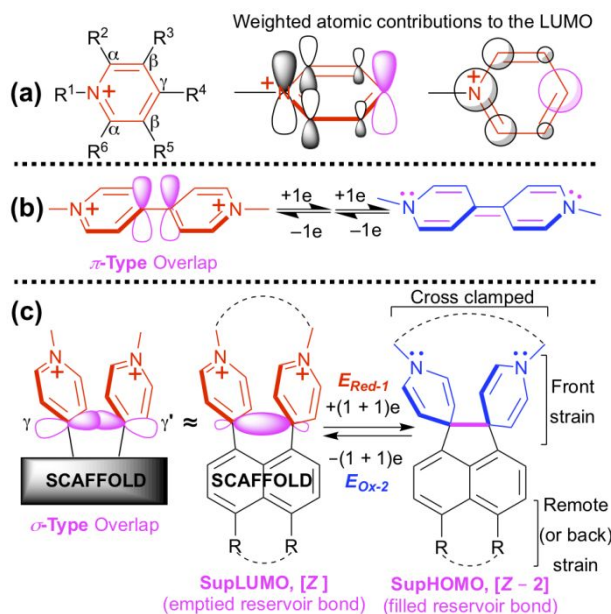


Chart 2. Molecular design of “structronic” prototypes: organizing electro-structural synergy. (a) Pictorial representation of the weighted atomic contributions (p_z atomic orbitals, AOs) to the LUMO of a pyridinium ring with emphasis on the large contribution of the C(γ) position. (b) Representation of the *in-plane* π -overlap between p_z AOs of the two C(γ) atoms of native MV²⁺, which form the basis of the second interannular bond involved in the overall quinoidal electronic structure adopted by MV⁰ (following the stepwise two-electron reduction of MV²⁺). (c) Representation of the sigma-type, *out-of-plane*, overlap of p_z AOs of the C(γ) atoms within the three-dimensional super-electrophore (i.e. SupLUMO build-up) in the *structronic* context, leading to the formation of the elongated C_{sp3}-C_{sp3} reservoir bond following an apparent single-step two-electron transfer (SupHOMO).

Connected at positions 1- and 8- of naphthalene (Chart 2), the two pyridinium units within the super-electrophore are anticipated to have their C(γ) carbon atoms in close vicinity, lying at a distance ($d(\text{C}(\gamma)\text{-C}(\gamma'))$) smaller²⁰ than the sum of their van der Waals (vdW) radii ($1.70 \times 2 = 3.40$ Å).²¹ This critical short contact serves to maximize orbital interaction (overlap) between the two rings at precisely the C(γ) sites where the LUMO of each pyridinium component has a large contribution (Chart 2a & 2c). In other words, instead

1
2
3 of the *in-plane* π -type delocalization that typically takes
4 place within the archetypal reference molecule MV^{2+} (Chart
5 2b), an *out-of-plane* sigma-type overlap of the LUMOs of the
6 two pyridinium building blocks is targeted as a result of
7 their *three-dimensional* pre-organization (Chart 2c).²² This
8 new bonding, virtual "supramolecular"²³ orbital generated
9 within the covalent assembly is in fact the LUMO of the whole
10 dicationic super-electrophore and its key feature. This
11 orbital that translates the electro-structural synergy is
12 herein referred to as the *SupLUMO*. This *SupLUMO* of the native
13 ($[Z] = 2+$) super-electrophore is to be filled upon two-
14 electron reduction thus leading to the desired *electron-*
15 *reservoir bond*, which incidentally corresponds to the *SupHOMO*
16 of the two-electron reduced ($[Z - 2] = 0$) super-
17 electrophore.²⁵

18
19
20
21
22
23
24
25
26
27
28
29 In order to assess the impact of the tailor-made
30 supramolecular assembly (*i.e.* the inner *askew* stacking of
31 electrophoric components) on pyridinium electrochemistry and
32 to investigate the process of strained-bond formation (and
33 breaking), we synthesized and studied, in parallel, the mono-
34 pyridinium assembly 1^+ and 4,4'-(naphthalene-1,8-diyl)bis(1-
35 methylpyridin-1-ium), 2^{2+} , the latter being a prototypical
36 super-electrophore for electron storage (see Chart 3). For
37 both 1^+ and 2^{2+} , structural characterization in the solid-state
38 (single-crystal X-Ray diffraction) and in solution (1H and ^{13}C
39 NMR) were carried out as well as the study of their
40 electrochemical and in-situ spectroelectrochemical (SEC)
41 properties, probing their electronic (UV-vis-NIR) and
42 vibrational (FTIR) characteristics. Experimental findings
43 were advantageously combined with molecular modeling using
44 DFT and TD-DFT. Further, in order to unambiguously establish
45 the number of electrons involved in the observed redox
46 processes, the reference compound (1^+) and the prototypical
47
48
49
50
51
52
53
54
55
56
57
58
59
60

super-electrophore (2^{2+}) were both derivatized with ferrocenyl (Fc) group(s) as single-electron redox probe(s) (Fc⁺/Fc), giving 1Fc^+ and 2Fc^{2+} , respectively (see Chart 3). Last, we also synthesized and studied the cyclophane-like analogue of 2^{2+} referred to as 3^{2+} that is, *N,N'*-(*n*-butyl)-1,8-di(pyrid-4-yl)naphthalene, in order to assess the impact of an increase of front strain via cross clamping of the electrophoric components (Chart 2c and Chart 3) on electrochemistry and especially the magnitude and positioning for the electrochemical hysteresis (see also Section S25 and Figure S16 in SI). Beyond the frustration effect on electrostructural relaxation of the reduction product (3^0), this last super-electrophore is also anticipated to providing us with the opportunity of getting some insights into the questioned relevance of using a 2-electron/multicenter pseudo-pancake covalent bonding as electron reservoir.

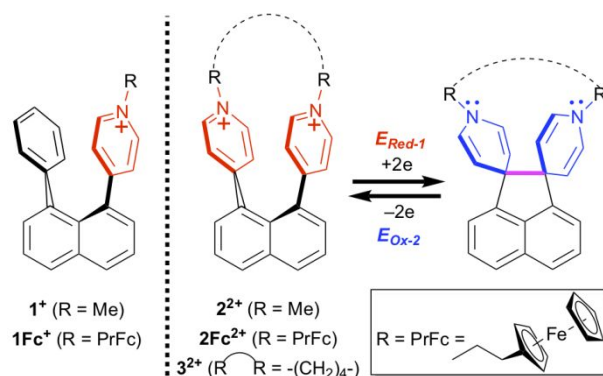


Chart 3. Molecular structures of the reference single-pyridinium electrophoric assembly, 1^+ , and of the two-pyridinium super-electrophores, 2^{2+} and 3^{2+} (hosting the bond that functions as a two-electron reservoir) along with ferrocenyl derivatives 1Fc^+ and 2Fc^{2+} . Syntheses and full characterization of various compounds are reported in SI (Section S28).

3. Results and discussion

For consistency reasons, all studies in solution (whether experimental or theoretical) were performed with acetonitrile (MeCN) solvent, using an implicit solvent model for calculations (see Experimental Section).

1
2
3 **3.1. Synthetic Strategy.** For the purpose of the present
4 study, besides the synthesis of the precursors of mono- and
5 di-pyridyl naphthalene via Suzuki-Miyaura coupling (see
6 Section S26 in SI), we have adopted a strategy that allows,
7 in a single step, the pyridinium formation (quaternarization)
8 or the Fc-derivatization via a saturated spacer that ensures
9 the electronic decoupling of redox-active subunits (i.e. Fc
10 and pyridinium). This approach, that relies on 3-
11 iodopropylferrocene²⁶ as a key synthon, is potentially
12 implementable with various kinds of compounds having pendant
13 pyridyl groups, when it is desired, for instance, to attach
14 redox probes to count the electrons involved in a redox
15 process while avoiding diffusion effects,^{14,16a,27} as is the case
16 here.
17
18
19
20
21
22
23
24
25
26
27
28

29 **3.2. Solid-State Characterization.** The molecular structures
30 of **1**[PF₆], **2**[PF₆]₂ and **3**[PF₆]₂ were determined by single-crystal
31 X-Ray diffraction (see Figure S1 and Section S4 in SI).
32 Analysis of the solid-state structure of **2**²⁺ confirms that the
33 two pyridinium rings connected at positions 1- and 8- of the
34 naphthalene scaffold are not stacked in a strictly parallel
35 fashion but are askew arranged.
36
37
38
39

40 The fact that distortion of molecular backbones is observed
41 in both **2**²⁺ and **1**⁺ regardless of the charge they hold in their
42 native form, indicates that steric hindrance rather than
43 adverse electrostatic repulsion (case of **2**²⁺) primarily
44 governs the overall structural features, as expected. This
45 finding agrees with previous results derived from the study
46 of congested polyacenes.^{17,28} Interestingly, and as expected,
47 the bridging of electrophoric subunits in **3**²⁺ via their N_{pyridinio}
48 atoms is found to improve the cofacial layout of the
49 pyridiniums (better pre-organization), enforcing the
50 naphthalene scaffold to decreasing its distortion, as
51
52
53
54
55
56
57
58
59
60

1
2
3 reflected by ABCD and θ angles, which amount to 2.78° , and
4 13.49° , respectively (see Figure S1 in SI).

5
6 A key parameter, especially for 2^{2+} and 3^{2+} , is the C(γ)-C(γ')
7 distance (see Chart 2c and $d(\text{C}(\gamma)\text{-C}(\gamma'))$) in Figure S1). From
8 single-crystal X-ray crystallography of **2** in the native state
9 (i.e. 2^{2+}), which contains two molecular assemblies per
10 asymmetric unit, a single distance is found to be shorter
11 than 3.4 \AA , which is indeed $d(\text{C}(\gamma)\text{-C}(\gamma'))$: $2.993 \text{ \AA} / 3.012 \text{ \AA}$,
12 as expected. On the contrary, three couples of atoms are
13 found to be in close contact within 3^{2+} , thereby satisfying
14 the vdW criterion of a 3.4 \AA maximum separation distance: the
15 $d(\text{C}(\gamma)\text{-C}(\gamma'))$, 2.958 \AA , and the two $d(\text{C}(\beta)\text{-C}(\beta'))$ atom pairs:
16 3.146 \AA and 3.291 \AA . It is thus anticipated that bonding
17 interactions will be different in 2^0 and 3^0 . Even if the above
18 picture of inner structural features of super-electrophores **2**
19 and **3** in their native state ($[Z] = 2+$) are derived from
20 solid-state characterization, one can reasonably expect that
21 virtually identical (although averaged) distortions are
22 present in solution.

23
24 Overall, the combination of the steric front strain¹⁹ between
25 pendant pyridylium groups with the intrinsic torsional
26 flexibility of naphthalene scaffold,¹⁷ and the prominent
27 contribution of the C(γ) p_z orbitals to the LUMO, come
28 together to favor a *single* through-space short contact within
29 **2**. On the contrary, with supplementary cross clamping i.e.
30 within the cyclophane-like model **3**, an enforced inner pseudo-
31 stacking (characterized by the *almost* cofacial layout of
32 heteroaromatic rings) is observed, which results in *multiple*
33 short contacts that could lead to a 2-electron/n-center
34 covalent bonding upon reduction (see below).

35
36
37
38
39
40
41
42
43
44
45
46
47
48
49
50
51
52
53
54
55
56
57
58 **3.3. Molecular Modeling.** DFT calculations were performed to
59 gain further insight into the molecular geometries and
60

1
2
3 electronic structures (frontier molecular orbitals) of the
4 native and reduced forms of **1**, **2** and **3**.

5
6 Geometry optimization of **1**, **2** and **3** in their native forms,
7 although obtained using a continuum representation of the
8 solvent, accurately reproduces the salient geometrical
9 features observed in the solid-state as determined from
10 single-crystal X-ray crystallography. This finding is
11 reflected in the good agreement of calculated values with
12 experimental data for the above-defined geometrical
13 parameters - $d(C(\gamma)-C(\gamma'))$, ABCD torsion angles, θ , ϕ and τ
14 (vide supra and Figure S1 and Table S1.1 in SI).
15
16
17
18
19
20
21

22 The calculated LUMO of model compound **1**⁺ is essentially
23 localized on the pyridinium subunit, with major contributions
24 from the α and γ positions (Figure 1). For both **2**²⁺ and **3**²⁺,
25 the LUMO is localized on the *ensemble* made of the two
26 interplaying pyridinium subunits, with major contributions
27 from the C(γ)/C(γ') atoms. Indeed, the close proximity of the
28 two electrophoric components ($d(C(\gamma)-C(\gamma'))$ *calculated*
29 *distance* = 3.039 Å and 2.983 Å) result in the through-space
30 bonding interaction (sigma-type overlap) between the p_z
31 orbitals of the C(γ) and C(γ') atoms. From the standpoint of
32 electronic structure, the lowest unoccupied "molecular"
33 orbital of **2**²⁺ and **3**²⁺ characterizes this *two-pyridinium*
34 *ensemble* as a *unified assembly*,²³ which we may refer to as the
35 necessary *SupLUMO* feature of the super-electrophore defined
36 in Section 2. Owing to the cross-conjugated nature of the
37 unsaturated naphthalene scaffold with 1,8-connectivity,²⁹ it
38 is most likely that the through-space supplementary bonding
39 interaction in dipyridinium species directly explains the
40 lower energy calculated for their *SupLUMO* (*En.* = -3.14 eV and
41 -3.30 eV for **2**²⁺ and **3**²⁺, respectively) as compared to the
42 energy calculated for the LUMO of **1**⁺ (*En.* = -2.73 eV).
43
44
45
46
47
48
49
50
51
52
53
54
55
56
57
58
59
60

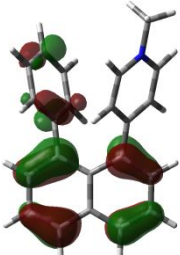
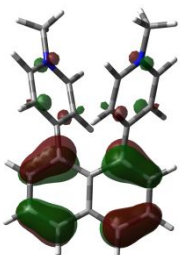
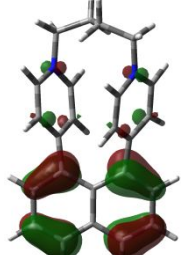
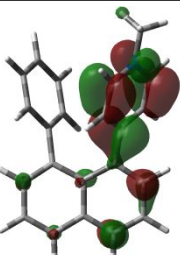
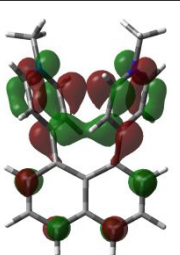
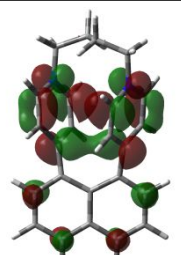
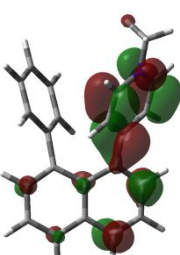
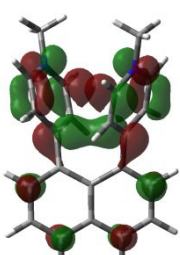
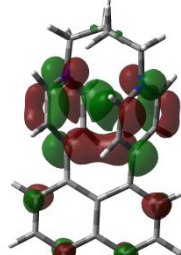
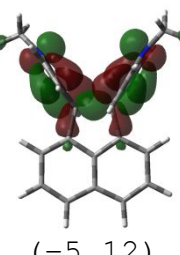
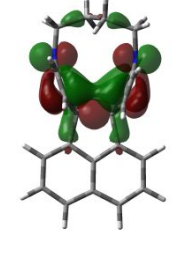
	1 (Energy / eV)	2 (Energy / eV)	3 (Energy / eV)
HOMO [Z]	 (-6.54)	 (-7.01)	 (-7.10)
LUMO [Z]	 (-2.73)	 (-3.14)	 (-3.30)
SOMO [Z - 1]	 (-3.62)	 (-3.95)	 (-4.03)
HOMO [Z - 2]	-	 (-5.12)	 (-5.11)

Figure 1. Relevant molecular orbitals for single-, **1**, and double- **2/3** pyridinium electrophores in native [Z], singly reduced [Z - 1] and doubly reduced [Z - 2] forms. These frontier MOs were calculated using the PBE0 exchange-correlation functional and are plotted with an iso-contour value of 0.04. The corresponding orbital energies are also given in eV.

Concerning the reduced species, it appears that structural reorganization upon reduction/oxidation is neither of the

1
2
3 same type nor of the same magnitude for $\mathbf{1}^+$ (see SI, Section
4 S8.2), $\mathbf{2}^{2+}$ and $\mathbf{3}^{2+}$ (Figure S2 in SI). For both $\mathbf{2}^{2+}$ and $\mathbf{3}^{2+}$, the
5 optimized geometry is to various extents characterized by a
6 distortion of the electrophoric subunits, with a decrease of
7 the $C(\gamma)-C(\gamma')$ distance. This configuration is a result of the
8 hybridization change of $C(\gamma)$ atoms from sp^2 to sp^3 , reflecting
9 the formation of the inter-pyridinium bond. As compared to
10 the length of the analogous covalent bond $d(C_{sp^3}-C_{sp^3})$
11 calculated in ethane (1.524 Å vs. 1.535 Å experimentally
12 measured by X-ray diffraction) or, more pertinently, in
13 acenaphthene (1.558 Å; Table S2 in SI), the calculated bond
14 between the two $C(\gamma)$ atoms is significantly elongated, thereby
15 confirming its relative weakness. Typically, in the case of
16 $\mathbf{2}^0$, it is estimated that the length of this electrochemically-
17 formed strained bond is 1.647 Å ($d(C_{sp^3}-C_{sp^3})$ calcd.) and is
18 characterized by an associated harmonic stretching force
19 constant which is about 70% that of a usual C-C sigma bond
20 (see Table S2 in SI). In fact, as is the case for the
21 *SupLUMO*, the spatial expanse of the HOMO naturally
22 encompasses the electrophoric components. The bond-length
23 alternation (BLA) pattern computed for the heterocyclic
24 fragments in going from $\mathbf{2}^{2+}$ to $\mathbf{2}^0$ (Table S1.1 in SI), namely
25 the shortening of $d(C(\alpha)-C(\beta))$ (from 1.377 to 1.347 Å) with
26 concomitant elongation of $d(N-C(\alpha))$ (from 1.348 to 1.382 Å)
27 and $d(C(\beta)-C(\gamma))$ (from 1.348 to 1.506 Å), reflects the
28 emerging quinoidal structure that develops in $\mathbf{2}^0$.^{16b} This loss
29 of aromaticity of the pyridinium rings is indicative of their
30 actual involvement in the reduction.^{16b} For consistency, we
31 found it more convenient to refer to the HOMO of super-
32 electrophore $\mathbf{2}$ in its [$Z - 2$] state (i.e. $\mathbf{2}^0$) as the *SupHOMO*.
33 The observation that the *SupLUMO* of $\mathbf{2}^{2+}$ and the *SupHOMO* of $\mathbf{2}^0$
34 essentially have the same spatial expanse and involve
35 essentially the same part of the super-electrophoric assembly
36
37
38
39
40
41
42
43
44
45
46
47
48
49
50
51
52
53
54
55
56
57
58
59
60

1
2
3 further substantiates the notion of an "electron reservoir"
4 (i.e. that the electrons are removed from the same place
5 (*SupHOMO*) that they were initially stored (*SupLUMO*)).
6

7
8 At this point, we recall that multi- $[n]$ -center ($n > 2$)
9 delocalization of like charges is an efficient means to
10 minimize adverse "on-site" Coulomb repulsion, which can be
11 achieved here via the extension of the bonding *SupLUMO* beyond
12 the two primarily-concerned $C(\gamma)$ centers. This is indeed
13 achieved here due to the involvement of the $C(\gamma)$ p_z AOs in (i)
14 the parent LUMOs of pyridinium units (in-plane π -type
15 overlap), and (ii) in the through-space interannular bonding
16 interaction (out-of-plane sigma-type overlap). If what we
17 define as the "reservoir" is restricted only to the
18 interannular component, the spread of the *SupLUMO/HOMO* onto
19 the pyridinium moieties can be considered as "leaking" of
20 this reservoir. Through this leaking, the reservoir itself
21 hosts less than two electrons, contributing to its weakened
22 nature. Alternatively, if we define the reservoir as an
23 assembly comprising both pyridinium units together with the
24 interannular bond, the formation/cleavage of the interannular
25 bond itself is therefore the tipping element that regulates
26 the function of the electron reservoir assembly. For further
27 general considerations concerning the quantum mechanical
28 description of the reservoir bond see SI (Section S7.2) and
29 for what concerns the optimized geometry and fate (such as
30 dimerization) of the singly-reduced mono-electrophoric
31 reference species (**1**[•]), see SI (Section S10.2).
32
33

34
35 Now, it is worth considering the case study of **3**. Within **3** in
36 its native state (**3**²⁺), the pyridinium rings are not strictly
37 cofacial, but adopt canted position towards each other, such
38 that the critical vdW close contact at sites γ/γ' is
39 preserved. It remains nonetheless that β/β' sites are also
40 found lying at distances smaller than 3.4 Å. Beyond
41
42
43
44
45
46
47
48
49
50
51
52
53
54
55
56
57
58
59
60

1
2
3 accurately reproducing above-mentioned experimental
4 interatomic distances, molecular modeling reveals that in its
5 doubly-reduced state ($\mathbf{3}^0$), the cyclophane-like super-
6 electrophore exhibits three ($1 \gamma/\gamma' + 2 \beta/\beta'$) bonding
7 interactions (see Table S1.2 in SI) as a result of the double
8 cross clamping of the two heterocycles ensured by the
9 butylene bridge and the newly formed γ/γ' bond. This means
10 that there is a 2-electron/6-center covalent pancake bonding
11 network within $\mathbf{3}^0$ instead of a regular 2-electron/2-center
12 covalent bond, as is the case within $\mathbf{2}^0$. This finding explains
13 why the electrochemically formed elongated γ/γ' bond is
14 paradoxically characterized by a force constant ca. 30%
15 larger than that computed for the C-C sigma bond of ethane
16 while this γ/γ' bond is even more elongated (i.e. weakened)
17 than that in $\mathbf{2}^0$ (i.e. 1.671 Å versus 1.647 Å; cf. also IR
18 frequencies: 854 cm^{-1} vs. 891 cm^{-1} , respectively; Table S2). In
19 fact, the calculation mode of the force constant (see
20 Experimental Section in SI), that involves ancillary bonding
21 interactions (pancake bonding), explains the greater value of
22 the γ/γ' force constant associated to $\mathbf{3}^0$ as compared to that
23 of $\mathbf{2}^0$.

24
25 From the standpoint of molecular design, it follows from this
26 finding that choosing a "pancake" bond¹⁰ as electron reservoir
27 is not relevant if one envisions relying on a mechanical
28 stress to exert a (remote) control of the
29 charging/discharging process of the structronic functional
30 assembly (i.e. the formation/cleavage of the reservoir bond
31 on demand). This is not only due to the increase of the
32 effective force constant associated to the reservoir bond
33 (see Table S2 in SI), but is also related to the low
34 magnitude of the redox-induced electro-structural relaxation
35 ("breathing") that limits the degree of freedom for
36 mechanical interplay (as compared to $\mathbf{2}$). These are the major
37
38
39
40
41
42
43
44
45
46
47
48
49
50
51
52
53
54
55
56
57
58
59
60

1
2
3 justifications for the selection of a 2-electron/2-center
4 bond as electron reservoir (see Section 2 devoted to
5 molecular design).
6
7

8 9 10 **3.4. Solution Study.**

11 **3.4.1. NMR Characterizations.** ^1H and ^{13}C NMR studies allowed
12 the investigation of the structural features of **2** (and **1**) in
13 CD_3CN solution in their native and chemically reduced forms.
14 The ^1H NMR signature of the dipyridinium derivative **2**²⁺
15 exhibits sharp signals of its protons at 298K indicating fast
16 fluxional changes at the NMR timescale that include
17 rotational motion of the two pyridinium rings and backbone
18 distortion of the naphthalene scaffold. As a result, **2**²⁺
19 exhibits an averaged C_{2v} symmetry in solution at room
20 temperature. After reduction of **2**²⁺ in CD_3CN solution with
21 sodium amalgam, $\text{Na}(\text{Hg})$ ($E^{0'}$ = -1.95 ± 0.01 V vs SCE in MeCN),³⁰
22 the recorded ^1H NMR spectrum also showed sharp signals, which
23 is indicative of the diamagnetic nature of **2**⁰, resulting from
24 the spin pairing (*i.e.* the antiferromagnetic coupling) of
25 heterogeneously transferred electrons. The two doublets at
26 8.31 and 7.73 ppm, ascribed to protons α and β in the native
27 form, are now observed at 6.01 and 4.17 ppm, lying in the
28 frequency region of ethylene compounds. These noticeable up-
29 field shifts ($\Delta\delta$), that amount to 2.30 and 3.56 ppm,
30 respectively (see Figure 2), are consistent with the loss of
31 aromatic structure for the two pyridiniums, which adopt a
32 quinoidal structure upon reduction. Further support stems
33 from the ^{13}C NMR experiment thanks to the sensitive chemical
34 shift of the $\text{C}(\gamma/\gamma')$ carbon nuclei, switching from the
35 aromatic frequency domain (δ = 160.1 ppm) in the native form,
36 **2**²⁺, to the aliphatic region (δ = 60.1 ppm) in the two-
37 electron reduced form **2**⁰, corresponding to a tremendous - yet
38 feasible - change in the chemical shift of 100 ppm (see
39
40
41
42
43
44
45
46
47
48
49
50
51
52
53
54
55
56
57
58
59
60

Figure S4 in SI). This observation is fully consistent with outcomes of ab-initio calculations that predict a change in the chemical shift, $\Delta\delta$, of 102.9 ppm for C(γ) (from 172.2 for 2^{2+} to 69.3 ppm: see Figure S4 in SI). This upheaval accurately reflects the change of hybridization of the C(γ/γ') carbon atoms from sp^2 to sp^3 that accompanies the electrochemically gated interannular covalent bond formation.³¹ In addition, through variable temperature NMR experiments we probed the stability of the newly formed 5-membered ring. Even at 333 K, no signal change or broadening (for instance, from a homolytic rupture of the new $C_{sp^3}-C_{sp^3}$ bond) was observed that could be attributed to intervening paramagnetic species. In fact, we will show below that the singly reduced radical intermediate cannot accumulate because of potential inversion³² (Section 3.5.2.2). Not only is the radical cation too short-lived compared to characteristic time of NMR (around a few seconds) but also observation that no radical species could be detected upon heating is informative regarding the relative robustness of the reservoir bond.

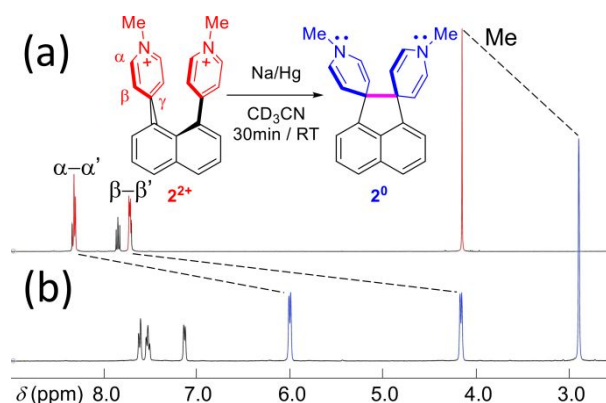


Figure 2. ^1H NMR spectra (400 MHz, CD_3CN , 298 K) of $2[\text{PF}_6]_2$ ($c = 10^{-2}$ mol L^{-1}) before (a) and after (b) chemical reduction, showing the diagnostic chemical shift of the H(α, α'), H(β, β') and N-Me protons of the electrophoric subunits; See also Section S29 in SI.

As far as the native form of the reference species $1[\text{PF}_6]$ is concerned, similar conclusions can be drawn from the ^1H and ^{13}C

1
2
3 NMR spectra regarding their fluxional (and averaged)
4 structures. However, contrary to the previous case, after
5 reduction of **1**[PF₆] in CD₃CN with Na/Hg, a more complex
6 spectrum is obtained (Figure S5) where protons of the
7 scaffold are more affected than those of pyridinium (see
8 Section S12.2), corresponding to a mixture of compounds among
9 which is the α - α (i.e. 2-2; Table S3 in SI) dimer (**1**)₂ that
10 is computed to be the most stable (see Table S4). Once again,
11 no effect ascribable to the presence of radical **1**[•] could be
12 evidenced. In fact, upon chemical reduction, whether
13 considering the cases of **1**[PF₆] or **2**[PF₆]₂, there is sufficient
14 time for chemistry to fully develop, which is not necessarily
15 the case with potentiodynamic electrochemical methods.
16
17
18
19
20
21
22
23
24
25
26
27

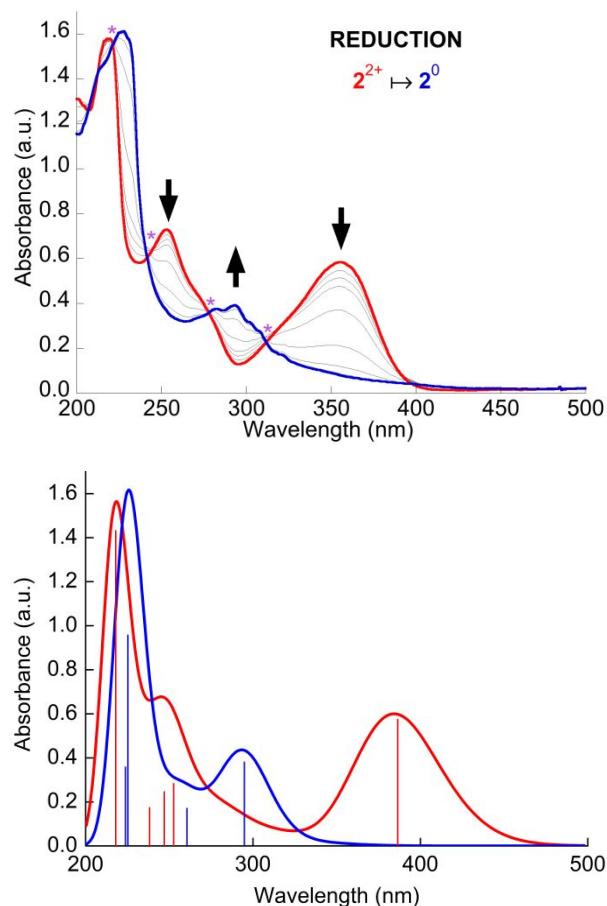
28 **3.4.2. In situ Spectroelectrochemical (SEC) Studies.**

29 Spectroelectrochemistry has the twofold advantage over its
30 chemical counterpart (e.g. the use of Na/Hg amalgam or
31 cobaltocene for reduction purposes) that the potential energy
32 of electrons as "reactants" can be continuously varied and
33 their availability controlled over time. Great assets of SEC
34 stem from the potential control of electron availability,
35 that is, the monitoring of a given redox process. In this
36 sense, the probed phenomena are not necessarily the same as
37 those observed by chemical means.
38
39
40
41
42
43

44 The UV-vis-NIR electronic absorption SEC study was performed
45 with 1 millimolar solutions of **1**[PF₆] and **2**[PF₆]₂ in 0.1M
46 TBAPF₆ in MeCN (Figure 3-top). Regarding the electronic
47 spectrum of **2**[PF₆]₂, three main absorption bands are observed
48 in the near UV region that are characterized by maxima at 221
49 nm, 253 nm and 357 nm. These absorption features are
50 accurately reproduced by TD-DFT calculations (*vide supra*)
51 that allowed the assignment of electronic transitions (Figure
52 3-bottom). The first two higher-energy bands (with simulated
53 maxima at 218 and 247/253 nm) are π - π^* transitions centered
54
55
56
57
58
59
60

1
2
3 on the naphthalene scaffold and on the pyridinium subunits,
4 respectively (see Table S6 and Figure S8 in SI). Most
5 importantly, the third, lowest-lying band (i.e. the red-edge
6 feature), calculated at 386 nm, is assigned to a single
7 electronic transition of HOMO-*SupLUMO* character,
8 demonstrating dominant (99 %) charge transfer (CT) character
9 from the electron-rich naphthalene moiety to the virtual
10 *SupLUMO*. This latter is *specific* to the two-pyridinium
11 "supramolecular" assembly (see Table S6 and Figure S8).
12 Indeed, as far as the lowest-lying virtual MO of the super-
13 electrophore is concerned, the two heteroaromatic moieties
14 are essentially through-space coupled, with virtually no
15 electronic interaction mediated through the bonds of the
16 naphthalene scaffold (see Figure 1), insofar as it behaves as
17 a cross-conjugated platform when considering the 1,8-
18 connectivity.²⁹ This CT band is therefore a diagnostic feature
19 supporting the existence of the target *SupLUMO*. The spectrum
20 of the two-electron-reduced species, **2**⁰, characterized by only
21 two major absorption bands at 228 and 295 nm, is obtained
22 upon varying the applied potential down to -1.20 V (vs.
23 quasi-reference electrode Ag/AgCl). As is the case for the
24 native state, the TD-DFT simulated spectrum of **2**⁰ compares
25 very well with the experimentally recorded trace, with two
26 bands of calculated maxima at 224 and 295 nm, respectively.
27 Theory tells us that the latter results from a pure π - π^*
28 transition centered on the naphthalene unit, as confirmed by
29 the structured shape (vibrational progression) experimentally
30 observed for the lowest-energy band. The observation that the
31 lowest-energy band of CT nature, evidenced for **2** in its
32 native state, is no longer present in the spectrum of **2**⁰, is
33 in line with the concept that the two-pyridinium
34 electrophoric assembly switches from being electron-deficient
35 (within **2**²⁺) to electron-rich (within **2**⁰) upon reduction.
36 Lastly, we emphasize the isosbestic points at 215, 241, 279
37
38
39
40
41
42
43
44
45
46
47
48
49
50
51
52
53
54
55
56
57
58
59
60

1
2
3 and 311 nm observed during the course of the reductive SEC
4 experiment, and that the spectrum of the super-electrophore
5 in its native form (2^{2+}) is restored upon reoxidation, showing
6 the same isosbestic points (see Figure S6 in SI). This
7 observation is consistent with the below-established
8 electrochemical cyclability (i.e. chemical reversibility)
9 that relies on both processes of two-electron reduction and
10 oxidation (see Section 3.5.2.1). It is worth noting that the
11 results of the FTIR vibrational absorption (SEC) study
12 further substantiate outcomes of the UV-vis SEC by evidencing
13 the bond-length alternation (BLA) attached to the quinoidal
14 form of the reduced pyridylium components within 2^0 and by
15 confirming the chemical reversibility of the redox
16 transformation $2^{2+}/2^0$ (see Section S21 in SI).
17
18
19
20
21
22
23
24
25
26



56
57 **Figure 3.** (Top) Spectroelectrochemical UV-vis experiments of a solution
58 of 2^{2+} (red) in MeCN ($c = 1 \times 10^{-3}$ mol L⁻¹ with 0.1 M of TBAPF₆). The spectrum
59 of 2^0 (blue) is obtained after achieving potential of -1.2 V against
60 Ag/AgCl quasi-reference electrode (reduction process). Asterisks (*)

1
2
3 indicate isosbestic points. (Bottom) Simulated absorption spectra of $\mathbf{2}^{2+}$
4 (in red) and $\mathbf{2}^0$ (in blue). Spectra are obtained by convolution with
5 Gaussian functions centered at calculated absorption energies with a fixed
6 full width at half maximum of 0.45 eV. Intensities were normalized with
7 respect to the experimental peak at 360 nm.
8
9

10 Based on the remarkable agreement between the experimental
11 results recorded by UV-vis SEC and computed data obtained
12 from the TD-DFT modeling, we may confidently deduce that: (i)
13 the CT band identifies the *SupLUMO* in $\mathbf{2}^{2+}$, (ii) isosbestic
14 points indicate that there is a clean and direct
15 transformation of $\mathbf{2}^{2+}$ into $\mathbf{2}^0$, consistent with the single-step
16 build-up of the reservoir bond (in line with the NMR study,
17 Section 3.4.1). Furthermore, the overall chemical
18 reversibility of the electrochemical process is established
19 through the recovery of the starting absorption spectrum of
20 native $\mathbf{2}^{2+}$ upon re-oxidation of $\mathbf{2}^0$ (see Figures S6 and S7 in
21 SI).
22
23

24 Roughly the same overall behavior is observed in the case of
25 $\mathbf{1}^+$ even if spectral changes upon *in-situ* processes of
26 reduction and re-oxidation are less pronounced (in particular
27 regarding contributions from charge-transfer excitations)
28 than in the case of the dipyridinium derivative (see Figure
29 S9 in SI). This finding is not surprising: a single
30 electrophoric subunit rather than the "synergistic assembly
31 of two coupled pyridinium subunits" is involved. The observed
32 reversibility of the SEC behavior is consistent with the
33 electrochemical behavior (see below, Section 3.5.2.1), which
34 shows that, when formed as a minor reduction product at low
35 potential scan rate (i.e. $v \leq 0.225 \text{ V s}^{-1}$), the dimer is
36 indeed oxidatively cleaved (Ox-2 process in Figure 5-top) and
37 the starting electrophore, $\mathbf{1}^+$, is recovered. The presence of
38 isosbestic points (Figure S9) is compatible with the
39 formation of both the radical species ($\mathbf{1}^{\bullet}$) and the dimer $[\mathbf{1}]_2$,
40 to the extent that their calculated spectral signatures are
41 very similar (see Figures S9 and S10 in SI).
42
43
44
45
46
47
48
49
50
51
52
53
54
55
56
57
58
59
60

3.5. Mechanistic Study.

3.5.1. Potential Inversion and Bond Formation: Insights from Computational Modeling.

Comparison of the MOs represented in Figure 1 suggests that the process of interannular covalent bond formation, which occurs inside super-electrophores **2** and **3**, is fundamentally different from the bimolecular process of dimerization. The first added electron enters the *SupLUMO* and is delocalized across both pyridinium units (i.e. not localized on a single pyridinium as would be the case for a genuine "inner" sigma dimerization). Only a slight structural change is computed for the first electron transfer, whereas the second electron transfer is clearly accompanied by a pyramidalization of each of the two C(γ) atoms. This unambiguously confirms the change of their hybridization from sp^2 to sp^3 .

As regards the prototype two-pyridinium super-electrophore, **2**, the comparison of the respective energies (Figure 1) of the *SupLUMO*/[Z] (-3.14 eV), *SupSOMO*/[Z - 1] (-3.95 eV) and *SupHOMO*/[Z - 2] (-5.12 eV) reveals that stabilization energy attached to the second heterogeneous electron transfer ($\Delta E = -1.17$ eV) is greater than that attached to the first electron transfer ($\Delta E = -0.81$ eV). Bearing in mind that bond formation is usually considered a barrierless process,³³ this means that the second one-electron reduction process is expected to be "easier" than the first one. To some extent, this finding can be viewed as an indication of an inversion of potentials for the chemical bond formation, provided that one considers the super-electrophoric multicomponent system as a single electronic entity (this is justified by the through-space interaction of the two pyridiniums, which gives rise to the *SupLUMO*). This inversion is consistent with observation of a single-step two-electron reduction (see below, Red-1 in Figures 4 and 5). Now, the question is the extent to which

1
2
3 *the oxidative bond cleavage also leads to a similar inversion*
4 *of oxidation potentials.* Experimentally, one should therefore
5 observe a single two-electron oxidation. In fact, this is in
6 line with observation of the cyclic voltammograms of **2** (see
7 below, Figure 5-bottom) and comparison of the derived semi-
8 integrated neo-polarograms (see Figure S15 in SI). Brought
9 together, these findings suggest that, from a mechanistic
10 standpoint, both the bond formation and bond cleavage
11 processes are a result of potential inversion phenomena.

3.5.2. Mechanistic Insights into Potential Inversion of Bond Formation/Cleavage from Electrochemistry and Simulation of Cyclic Voltammograms.

24
25 **3.5.2.1. Electrochemical Study.** Electrophores **1⁺** and **2²⁺** were
26 derivatized with redox probes that undergo a monoelectronic
27 redox process ($n = 1$), namely ferrocene (Fc) units that are
28 appended via saturated propylene linkers at N_{pyridinio} atoms (**1Fc⁺**
29 and **2Fc²⁺** in Chart 3). Cyclic voltammograms (CVs) at a
30 stationary electrode and linear sweep voltammograms (LSVs) at
31 a rotating disk electrode (RDE) are shown in Figure 4.
32 Comparison of the LSV wave heights for electrophores
33 identical to **1⁺** and **2²⁺** and that of Fc probes confirms that the
34 number (n) of electrons involved in the reduction processes
35 (Red-1) is equal to the number of Fc units, that is, $n = 1$
36 and 2 for **1Fc⁺** and **2Fc²⁺**, respectively.³⁴ CVs of **1Fc⁺** and **2Fc²⁺**
37 reveal sizably different behaviors (Figure 4). For **1Fc⁺**, one
38 quasi-reversible redox process (Red-1/Ox-1) at -1.278 V ³⁶ is
39 observed along with an oxidation process (Ox-2) in the return
40 scan at $E_{\text{pa-(Ox-2)}} = -0.362 \text{ V}$, which is characterized by a much
41 smaller peak current. For **2Fc²⁺**, the reduction (Red-1) is an
42 irreversible process that occurs at a more positive potential
43 than for **1Fc⁺** ($E_{\text{pc-(Red-1)}} = -1.002 \text{ V}$), which is also accompanied
44 in the return scan by an irreversible oxidation process ($E_{\text{pa-(Ox-2)}}$

2) = -0.095 V) that manifests itself as a well-defined broad peak characterized by a current intensity lower than the reduction peak (Red-1). The irreversible oxidation process (Ox-2) is not present in the first anodic scan (starting from -0.6 V to +1.0 V) and appears only after the reduction process (Red-1) is complete. Such a sequence-dependence indicates that Ox-2 is an electrochemical-chemical (E-C) process related to the oxidation of a reduction product of Red-1, which therefore also involves an E-C process (see below). Further, the anodic shift of the Red-1 reduction potential ($\Delta E_{Red-1} = +0.276$ V) in going from $1Fc^+$ to $2Fc^{2+}$ is consistent with the presence of an interaction between the two pyridinium units within $2Fc[PF_6]_2$ and thus within $2[PF_6]_2$.

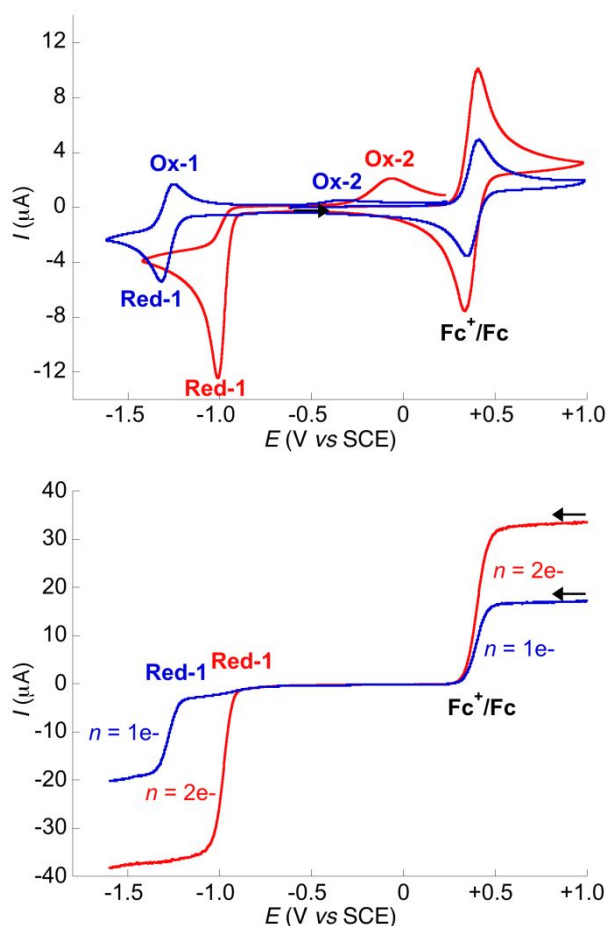


Figure 4. Cyclic voltammetry (top) and rotating disk electrode (RDE) experiments (bottom) of $1Fc[PF_6]$ (blue traces) and $2Fc[PF_6]_2$ (red traces) solutions ($c \approx 5 \times 10^{-4}$ mol.L⁻¹ in MeCN with 0.1 M of TBAPF₆) both recorded at scan rate v of 0.1 V s⁻¹ and rotation speed r of 2000 rpm.³⁷

In order to get further insight into the very nature of Ox-2 processes observed for one- and two-electron-reduced electrophores $\mathbf{1}^+$ and $\mathbf{2}^{2+}$, we performed a potentiodynamic study as a function of the potential scan rate (v) (Figure 5).

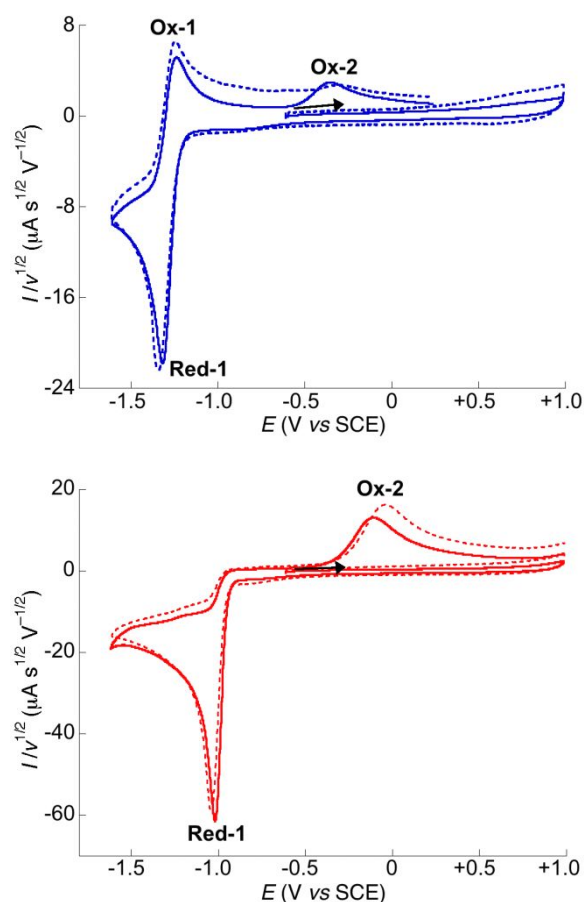


Figure 5. Cyclic voltammograms of $\mathbf{1}[\text{PF}_6]$ (top; blue traces) and $\mathbf{2}[\text{PF}_6]_2$ (bottom; red traces) solutions ($c \approx 5 \times 10^{-4} \text{ mol L}^{-1}$ in MeCN with 0.1 M of TBAPF₆) recorded at 0.1 V s^{-1} (solid line) and at 0.625 V s^{-1} (dashed line). CV traces are normalized against the square root of the potential (applied voltage) scan rate v .³⁸

From comparison of CVs recorded at 0.1 V s^{-1} and 0.625 V s^{-1} , one notices that the main difference stems from the status of the Ox-2 process, which becomes virtually indiscernible at higher scan rate for $\mathbf{1}^+$ (ca. $v > 0.225 \text{ V s}^{-1}$) while it remains virtually unchanged for $\mathbf{2}^{2+}$ (this latter behavior was actually verified for v values of up to 1000 V s^{-1} using an ultramicroelectrode setup).³⁹ In other words, the Ox-2

1
2
3 processes are clearly different in nature for redox-active
4 species $\mathbf{1}^+$ and $\mathbf{2}^{2+}$ and the insensitivity to potential scan rate
5 observed for $\mathbf{2}^{2+}$ clearly points towards a fast chemical
6 process, and more precisely a process inner to the super-
7 electrophore (i.e. the formation of the reservoir bond). In
8 this case, it is worthwhile establishing the number (n) of
9 electrons involved in the Ox-2 process of $\mathbf{2}^0$. This number is
10 typically derived from semi-integration (i.e. convolution)⁴⁰
11 of the CV of $\mathbf{2}^{2+}$ recorded at $v = 0.1 \text{ V s}^{-1}$ (see Figure S15 in
12 Section S25.1 of SI), which here shows that n is the same for
13 the reduction (Red-1) and the return scan (Ox-2) processes,
14 i.e. $n = 2$, as expected. Besides, Section S25.1 also reports
15 the comparison of electrochemical behaviors of $\mathbf{2}$ and $\mathbf{3}$.

16
17
18
19
20
21
22
23
24
25
26 Conversely to $\mathbf{2}$ (and $\mathbf{3}$), the quasi-reversibility of the
27 Red-1 process together with the scan rate dependence of Ox-2
28 in the case of single-pyridinium electrophore ($\mathbf{1}^+$) are
29 straightforwardly explained by intervening intermolecular
30 process that requires the formation of pairs of reactive
31 species (singly-reduced electrophores i.e. radicals $\mathbf{1}^{\bullet}$). This
32 is the well-documented dimerization process⁴¹⁻⁴⁴
33 (electrochemical-chemical - EC_{dim} - mechanism) here giving most
34 likely the *ortho-ortho* dimers $[\mathbf{1}]_2$, consistently with
35 computational outcomes (see SI, Section S10.2) as well as
36 observations out of the NMR study (see Section 3.4.1 and
37 Figure S5).

3.5.2.2. Electrochemistry and CV Simulation.

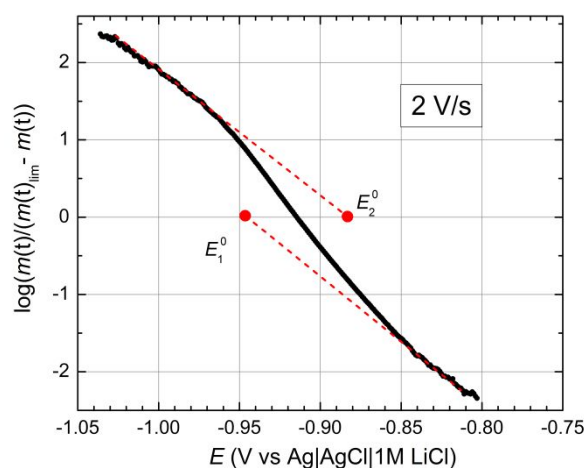
38
39
40
41
42
43
44
45
46
47
48
49
50 Fast electron transfer followed by the dimerization of a
51 radical intermediate is a common mechanism often encountered
52 in the reduction of pyridinium-based derivatives.
53 Dimerization is a bimolecular process, which is characterized
54 not only by a positive shift of the redox potential of the
55 product, as compared to that of parent single-pyridinium
56
57
58
59
60

1
2
3 "monomers", but is also dependent on the bulk concentration.⁴⁵
4
5 An archetypal example is the more than centennial synthetic
6
7 route to methyl viologen (**MV**).⁴⁶ The theory and application of
8
9 the reduction-dimerization process was developed by
10
11 Koutecký,⁴⁷ Blunt,⁴⁸ Olmstead⁴⁹ and Savéant.⁵⁰ However, above-
12
13 described experiments unambiguously established that
14
15 reduction of 2^{2+} (Red-1 in Figures 4 and 5) is not a one- but
16
17 a *two-electron* process (see Section 3.5.2.1). Features, which
18
19 distinguish the redox mechanism of 2^{2+} from bimolecular
20
21 dimerization are (i) the two-electron reduction, (ii) the
22
23 independence of redox potentials on the bulk concentration,
24
25 (iii) observation of Ox-2 process at higher scan rates, (iv)
26
27 spectroscopic proof of the bond formation inner to the super-
28
29 electrophore (Section 3.4). These features confirm that the
30
31 observed reduction mechanism of 2^{2+} is consistent with an
32
33 inner process, namely the electrochemical σ -bond formation.
34
35 Therefore, *the reservoir-bond formation has nothing to do*
36
37 *with an ordinary bimolecular dimerization*. This agrees with
38
39 theoretical calculations that pointed to the inner bond
40
41 formation correlated with characteristic structural and
42
43 electronic rearrangements (Section 3.3). The heterogeneous
44
45 transfer of two electrons at apparently the same driving
46
47 force, *i.e.* at the same applied potential, implies that the
48
49 standard redox potentials E^0_1 and E^0_2 for the transfer of each
50
51 electron are either compressed (up to a coalescence) or even
52
53 inverted (Section 3.2). Detailed analysis of the current-
54
55 voltage dependence obtained by the cyclic voltammetry at
56
57 higher scan rates indeed confirms the potential inversion
58
59 phenomenon (as suggested in Sections 3.5.1 and 3.5.2.1). The
60
voltammogram using the glassy carbon electrode (see Section
S26-A in SI) and the scan rate of $2 \text{ V}\cdot\text{s}^{-1}$ (Figure S21) yields
similar semi-integrated "neo-polarograms" or "convolution
voltammograms" as those shown in Figure S15. The separate

1
2
3 semi-integration of each voltammetric half-cycle yields well-
4 defined waves (Figure S22) reaching a limiting value of the
5 semi-integral of the current, $m(t)_{\text{lim}}$,⁵¹ and thus enabling the
6 analysis of the wave shapes by the log-plot analysis:
7
8
9

$$10 \quad \log \frac{m(t)}{m(t)_{\text{lim}} - m(t)} \text{ vs. } E$$

11
12
13 The two-electron reduction yields the log-plot trace
14 featuring an S-shaped curve, having two linear asymptotes
15 with the same slope of 59 mV/decade, as is expected for two,
16 fast, one-electron transfers. This allows not only the
17 estimation of the two standard potentials, E°_1 and E°_2 , but
18 also provides the demonstration that these latter are
19 inverted (Figure 6). The difference $|E^{\circ}_1 - E^{\circ}_2| = 60$ mV is
20 obtained both at lower and at higher voltage scan rates (0.06
21 $\text{V}\cdot\text{s}^{-1} \leq v \leq 2 \text{ V}\cdot\text{s}^{-1}$). This insensitivity of the voltage
22 difference with respect to v was further verified by
23 numerical fitting of a series of voltammograms by application
24 of the finite difference techniques. Furthermore, it is worth
25 noting that the magnitude of the experimentally derived
26 potential inversion (ca. 60 mV) is in line with the
27 computational estimate (ca. 40 mV; see Section S7.3 in SI).
28
29
30
31
32
33
34
35
36
37
38

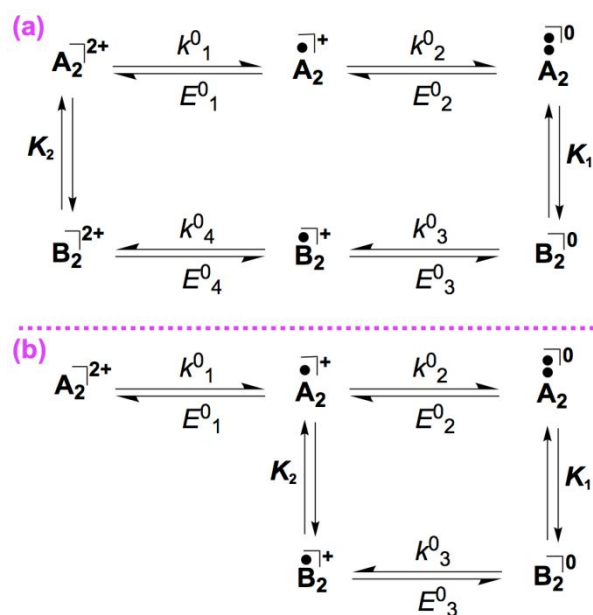


55 **Figure 6.** Log-plot analysis of semi-integrated neo-polarogram (Figure
56 S22) calculated for the reduction step (0.5 mM $\mathbf{2}^{2+}$ and TBAPF₆ 0.1M in MeCN,
57 glassy carbon electrode, scan rate 2 V s⁻¹). Extrapolation of two
58 asymptotes to y-axis = 0 yields two redox potentials for the first E°_1 and
59 the second E°_2 electron transfer step. The potential difference $|E^{\circ}_1 - E^{\circ}_2|$
60 is 60 mV.

1
2
3
4
5 An analogous log-plot analysis applied to the oxidation wave
6 (Ox-2) is not that straightforward. This peak, observed in
7 the return scan regardless of potential scan rates, is indeed
8 rather small due to the diffusion of the neutral σ -bonded
9 reduction product toward the bulk. The lack of a reduction
10 counterpart for the oxidation process Ox-2 of the σ -bonded
11 form indicates that this inner-sphere σ -bond cleavage is a
12 fast and irreversible process (see Section S26-B in SI). This
13 is in line with the assumption that the Ox-2 process
14 regenerates the electrophore in its starting (native) form,
15 **2²⁺**.

16
17 The digital simulation of CVs by finite difference methods
18 considered two possible reaction schemes differing in
19 sequences of electron transfers (E) and the chemical reaction
20 (C, here the σ -bond formation and cleavage). The overall
21 electrochemical reaction is usually referred to as an EEC
22 process and is represented in Chart 4a where **A₂²⁺** and **B₂⁰** stand
23 for **2²⁺** and sigma-bonded **2⁰**. Alternatively, the structural
24 change (*i.e.* the bond cleavage) could take place right after
25 the first electron withdrawal, as it is shown in Chart 4b.
26 The latter case would be termed an ECE mechanism. The
27 equilibrium constants and chemical rates are $K_1 = k_1/k_{-1}$ and $K_2 =$
28 k_2/k_{-2} .

29
30
31
32
33
34
35
36
37
38
39
40
41
42
43
44
45
46
47
48
49
50
51
52
53
54
55
56
57
58
59
60



23 **Chart 4.** Reaction scheme involving the two-electron reduction and re-
 24 oxidation with a coupled chemical reaction (EEC mechanism for both steps;
 25 top, (a)); The EEC mechanism applies for the reduction, whereas ECE
 26 pathway holds for the oxidation (bottom, (b)). The point is that for both
 27 (a) and (b) schemes, forward pathway to $\text{B}_2^{\bar{0}}$ is different from backward
 28 pathway, which is the *sine qua none* condition for obtaining
 29 electrochemical hysteresis supporting electron storage; k_n^0 are standard
 30 rate constants of heterogeneous electron transfers.

31
32
33 Since the digital simulation analysis of the oxidation wave
 34 allows unambiguously identifying of two redox potentials E'_3
 35 and E'_4 the reaction mechanism most likely involves the EEC
 36 scheme with potential inversion (Chart 4a) for both the
 37 reduction (Red-1) and the oxidation (Ox-2) steps. The fitting
 38 of voltammograms recorded over a wide range of v -values,
 39 usually confirms the nature of the reaction scheme.⁵² Both
 40 reaction mechanisms contain a large number of kinetic
 41 parameters and equilibrium constants. This raises issues
 42 regarding the reliability of fitting outcomes insofar as
 43 several combinations of adjustable parameters may give
 44 similar results. It is therefore worthwhile getting an
 45 estimate at least of some of the input parameters (see
 46 Section 3.5.2.1 and Section S26 in SI).

47
48
49 An example of calculated data that quite accurately fit
 50 experimental data is given in Figure S26 (see also Table S11
 51 in SI). Fitting indeed reasonably reproduced the i_a/i_c ratio
 52
53
54
55
56
57
58
59
60

(Figure S27), the potential differences ($E^0_1 - E^0_2$) = 71 mV and ($E^0_3 - E^0_4$) = 141 mV as well as fulfilling additional conditions stated in Section S26. Most importantly, not only did this simulation distinguish between E^0_3 and E^0_4 , it also demonstrated that *potential inversion is at work for the bond cleavage*, as is the case for the bond formation.

In summary, the combination of electrochemical experimental and fitted data indicates that both the reduction (Red-1) and the oxidation (Ox-2) obey the EEC mechanism given in Chart 4a. Finally, pathways for reduction and oxidation are however different with respect to the involved redox-active species (**A/B** in Chart 4a), thereby accounting also for the experimentally evidenced electrochemical hysteresis. Chart 5 explicitly summarizes the two-electron reduction/oxidation cycles operative, with a two-way potential inversion for super-electrophore **2** (and also **3**).

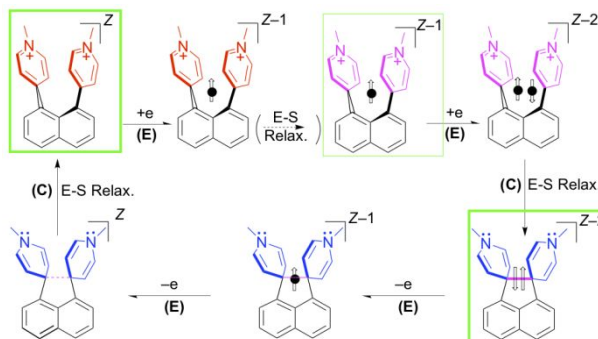


Chart 5. The pictorial representation of the mechanism underpinning the working principle of the structronic electrochemical paradigm thoroughly investigated in the present work. The functional assembly (**2**) referred to as a structronic prototype is akin to a kind of 3-dimensional **MV** ("3D-MV") but displaying an electrochemical behavior sharply different from that of the 2D, **MV** benchmark species.

3.6. Insights gained from other instances of electrochemically-gated Carbon-Carbon bonds within organic systems.

First of all, it's worth noting that, contrary to **3** that relies on cross clamping to tune electrochemical hysteresis (see Section S25.1 in SI), assemblies reported in this

1
2
3 section rely on two other steric constraints that are namely
4 the front strain as well as the back (remote) strain (see
5 Chart 2c). So, interestingly, there exist connections between
6 the applied field of molecular-based electrochromism,⁵³ that
7 is, the molecular-level optical switching (output) controlled
8 by an electrochemical input, and the basic research efforts
9 devoted to the exploration of "ultralong C-C bonds and of
10 their limits",^{54,55} that are, actually, beyond⁵⁶⁻⁵⁸
11 expectations.^{59,60} The above-mentioned connection stems from the
12 intriguing electrochemical phenomenon referred to as "Dynamic
13 Redox" (DyRex) behavior,^{54,55,61} also referred to as
14 "intramolecular switching of single bonds"⁶² (Chart S1 in SI).
15 Namely, it was shown that covalent assemblies properly
16 incorporating couples of redox-active units can give rise to
17 the formation of a (C_{sp3}-C_{sp3})⁶³ carbon-carbon bond that bridges
18 electrochemically active components following a reductive or
19 an oxidative process. For example, typically integrated
20 redox-active chromophoric units are trityliums,^{53,61,64} hetero-
21 tricyclic hydrocarbons,^{65,66} thiophenes,⁶⁷ or
22 octamethoxytetraphenylene.⁶⁸ Of particular interest is the
23 case of bis-acridinium assemblies (e.g. Chart S1a) that are
24 more or less tightly pre-organized with various semi-rigid to
25 rigid scaffolds, *i.e.* biphenyl, naphthalene, acenaphthene and
26 acenaphthylene.^{54,69} Structural evidences were collected from
27 crystallographic studies (single-crystal X-ray diffraction)
28 establishing (i) the reality of the elongated nature of the
29 newly formed C_{sp3}-C_{sp3} sigma bonds ($d(\text{C-C}) > 1.69 \text{ \AA}$ vs. 1.54 \AA
30 for ethane) and (ii) the existing relationship between these
31 bond-lengths and both the "front strain" due to inter-
32 electrophoric steric hindrance and the "back strain" giving
33 variously distorted scaffolds. Such experimental data are not
34 available from our own study in spite of our trials for
35 crystallizing **2**⁰. The important point here is that acridinium
36
37
38
39
40
41
42
43
44
45
46
47
48
49
50
51
52
53
54
55
56
57
58
59
60

1
2
3 is closely affiliated to pyridinium as regards its
4 electrochemical/electrophilic activity at the C(γ) site, that
5 corresponds to the C(9) position of the acridinium (Chart
6 Sla). However, they sharply differ in their reactivity at
7 either side of the N_{pyridinio} atom (i.e. *ortho* C(α) sites of
8 pyridinium motif). In the case of acridinium, the presence of
9 two edge-fused lateral rings, i.e. dibenzoannulation, at one
10 and the same time prevents from the above-mentioned
11 detrimental *ortho* reactivity (including nucleophilic
12 addition), and strengthens the chemical stability of the
13 pyridinium core (otherwise likely to undergoing ring
14 opening).⁵⁵ In fact, we were sharing in these respects the
15 same concerns as Suzuki and coworkers, especially about *ortho*
16 (C2 and C6) reactive positions of pyridinium.⁵⁴ Originally, we
17 were considering the "naked" pyridinium derivative (**2**²⁺) as a
18 non-optimized demonstrator compound, likely to be
19 subsequently improved by ensuring its *ortho* protection with
20 some bulky substituents. The present work demonstrates that
21 such a protection was, in fact, superfluous thanks to the
22 effects of the synergistic interplay of electrophoric units.
23 Although specifically implemented as a key-ingredient of the
24 design of structronic devices, this synergy was finally found
25 to be more efficient than initially planned i.e. its impact
26 on reactivity had been underestimated (Chart 2c). Indeed, we
27 found that the "SupLUMO" of **2**²⁺ was functioning as a genuine
28 attractor that diverts or traps the whole reactivity of
29 classical (i.e. isolated) pyridinium.
30 For a further thorough comparative discussion of Dyrex
31 systems with super-electrophores described in the present
32 work, see Section S27 in SI.

33 34 35 36 37 38 39 40 41 42 43 44 45 46 47 48 49 50 51 52 53 54 55 56 57 **4. Summary and Conclusions.** 58 59 60

1
2
3 The reactivity of pyridinium components within **2** (and **3**) was
4 found to be heavily impacted compared to that of naked
5 pyridinium or to a mono-pyridinium model species like **1**. The
6 synergistic interplay of the two electrophoric units allows
7 both (i) emergence⁷⁰ of the *SupLUMO*, which acts as a
8 "reactivity sink" towards the target reservoir-bond formation
9 inner to the super-electrophoric assembly and (ii), the
10 protection of the super-electrophore from side reactions,
11 like is intermolecular α -dimerization. The lack of reactivity
12 at α sites of these pyridinium moieties within the 3-*D*
13 structronic construct is reminiscent of that of the well-
14 known 2-*D* (roughly planar) covalent **MV** species (as a one-
15 electron redox shuttle or mediator). However, depending on
16 the nature of electrophores, the manner by which the two
17 electrons are transferred is sharply different, due to
18 fundamentally different working principles (electrochemical
19 paradigms). In the case of **MV**, the lack of reactivity of the
20 one-electron-reduced intermediate is basically due to
21 delocalization of this electron over the whole molecular
22 skeleton whereas in the case of **2** and **3**, it is rather related
23 to the transient nature of the one-electron-reduced species
24 due to potential inversion as well as its buried nature due
25 to the inner location of pivotal *SupLUMO*/*SupSOMO*. This latter
26 situation is due to inversion of electrochemical potentials
27 and, to a lesser extent, the lowered spin density at α -
28 positions as a result of its withdrawal towards the C(γ)
29 sites, hence the uncompetitive *intermolecular* dimerization.
30 Noteworthy, the *inversion of potentials* is demonstrated for
31 both the filling of the *SupLUMO* reservoir (two-electron
32 reduction with bond formation) and for the emptying of the
33 filled reservoir taking the form of the *SupHOMO* (two-electron
34 oxidation with bond breaking).
35
36
37
38
39
40
41
42
43
44
45
46
47
48
49
50
51
52
53
54
55
56
57
58
59
60

1
2
3 Finally, super-electrophore **2** which, at first, can be
4 regarded as the result of a rough design, turned out to be a
5 relevant demonstrator and a proof of the "structronics"
6 concept, in spite of its simplicity. This prototype has the
7 great asset of cost-effectiveness thanks to its low
8 engineering level as well as chemical robustness (see
9 Sections 3.4.1 and S27). These features both pertain to the
10 "Sustainocene" criteria.^{5,6b} Of course, there is still a long
11 way to go to reach truly workable devices that could enter
12 the marketplace. Indeed, it is now a matter of designing
13 electroactive molecular-based materials with a high density
14 of "structronic" elements so as to obtain workable storage
15 devices from the standpoint of charge-density. This could
16 possibly be obtained by grafting "structronic" assemblies at
17 the surface of conductive electrodes (e.g. graphene) or by
18 embedding these functional elements within a matrix of
19 conducting polymers or inside nanoporous conductive covalent
20 organic frameworks (COFs), using electricity of photovoltaic
21 origin. Actually, possible utilizations of super-
22 electrophores span from the field of solution organic
23 molecular chemistry (e.g. as new generation super-electron-
24 donors, SED,⁷¹ which are adjustable and electrochemically
25 rechargeable to deliver couples of redox equivalents) to the
26 field of electrochemical energy storage devices, thus
27 functioning as building blocks of organic⁷² or redox-flow⁷³
28 batteries. From the standpoint of homogeneous artificial
29 photosynthesis and, above all, of advanced Photochemical
30 Molecular Devices (PMDs),²⁴ it's worth bearing in mind that
31 what can be done electrochemically can be achieved
32 photochemically, provided that suitable photosensitizers are
33 involved. Thus, the "structronic" (+ photosensitizers)
34 functional component(s) can be associated with various
35 catalysts (whether molecular or nanoparticulate) and with
36 electron donors⁷⁴ (whether sacrificial or not) to give
37
38
39
40
41
42
43
44
45
46
47
48
49
50
51
52
53
54
55
56
57
58
59
60

1
2
3 molecular-level principles able to manage multi-photon/multi-
4 electron i.e. *photosynthetic* transduction processes.
5
6
7
8
9

10 **ASSOCIATED CONTENT**

11 **Supporting Information (SI):** Experimental Section; Complete
12 ref. 12; X-ray structures of **1**[PF₆], **2**[PF₆]₂ and **3**[PF₆]₂ along
13 with cif files; optimized geometries and electronic
14 structures of **1**, **2** & **3** in their various redox states; ¹³C
15 solution NMR (CD₃CN) of **2** after chemical reduction;
16 supplementary electrochemical studies of **2** and **3**;
17 complementary UV-vis-NIR and FTIR SEC experimental data along
18 with corresponding calculated data; further considerations
19 regarding electrochemical hysteresis of other known organic
20 redox systems with electrochemically triggered bond
21 formation/cleavage (DyRex systems); syntheses and full
22 characterization of the various compounds. The Supporting
23 Information is available free of charge on the ACS
24 Publications website.
25
26
27
28
29
30
31
32
33
34
35
36

37 **AUTHOR INFORMATION**

38 **Corresponding authors**

39 hyacinthe.randria@univ-paris-diderot.fr;
40 Ilaria.ciofini@chimie-paristech.fr;
41 magdalena.hromadova@jh-inst.cas.cz;
42 lubomir.pospisil@jh-inst.cas.cz
43 philippe.laine@univ-paris-diderot.fr
44
45
46
47

48 **ORCID**

49 Romana Sokolová: 0000-0003-1705-7401
50 Magdaléna Hromadová, : 0000-0002-3138-6917
51 Ilaria Ciofini: 0000-0002-5391-4522
52 Lubomír Pospíšil: 0000-0003-2543-2195
53 Henri-Pierre Jacquot de Rouville: 0000-0002-9508-6446
54 Hyacinthe Randriamahazaka: 0000-0002-8256-7486
55 Grégory Dupeyre: 0000-0002-4528-2481
56 Philippe P. Lainé: 0000-0001-7053-1833
57
58
59
60

Conflicts of interest.

The authors declare no competing financial interest.

Acknowledgment

Financial supports by the Grant Agency of the Czech Republic (18-04682S), and the Academy of Sciences of the Czech Republic (RVO: 61388955, 61388963), the Ministry of Education of the Czech Republic (Barrande project 7AMB15FR027), the French Ministries of Europe and Foreign Affairs (MAE) and of Advanced Education, Research and Innovation (MESRI) (PHC Barrande, 2015 project N° 34012SC), the European Research Council (ERC) under the European Union's Horizon 2020 research and innovation program (grant agreement No 648558) and the French National Research Agency, ANR ("E-StorIc" project : ANR-14-CE05-0002), are gratefully acknowledged.

Notes and references

- (a) Lorius, C.; Jouzel, J.; Ritz, C.; Merlivat, L.; Barkov, N. I.; Korotkevich Y. S.; Kotlyakov, V. M. A 150,000-year climatic record from Antarctic ice. *Nature*, **1985**, *316*, 591-596; (b) Barnola, J. M.; Raynaud, D.; Korotkevich, Y. S.; Lorius, C. Vostok ice core provides 160,000-year record of atmospheric CO₂. *Nature*, **1987**, *329*, 408-414; (c) Lorius, C.; Jouzel, J.; Raynaud, D.; Hansen, J.; Le Treut, H. The ice-core record: climate sensitivity and future greenhouse warming. *Nature*, **1990**, *347*, 139-145.
- Crutzen, P. J. Geology of mankind. *Nature*, **2002**, *415*, 23.
- (a) Service, R. F. Is It Time to Shoot for the Sun? *Science*, **2005**, *309*, 548-551; (b) Crabtree G. W.; Lewis, N. S. Solar energy conversion. *Physics Today*, **2007**, *60*, 37-42; (c) Lewis, N. S. Toward Cost-Effective Solar Energy Use. *Science*, **2007**, *315*, 798-801.
- (a) Kerr R. A.; Service, R. F. What Can Replace Cheap Oil—and When? *Science*, **2005**, *309*, 101; (b) Lewis N. S.; Nocera, D. G. Powering the planet: Chemical challenges in solar energy utilization. *Proc. Natl. Acad. Sci. U.S.A.*, **2006**, *103*, 15729-15735; (c) Armaroli N.; Balzani, V. The Future of Energy Supply: Challenges and Opportunities. *Angew. Chem., Int. Ed. Engl.*, **2007**, *46*, 52-66; (d) Pellegrin Y.; Odobel, F. Molecular devices featuring sequential photoinduced charge separations for the storage of multiple redox equivalents. *Coord. Chem. Rev.* **2011**, *255*, 2578-2593.
- Faunce, T. Towards a global solar fuels project—Artificial photosynthesis and the transition from anthropocene to sustainocene. *Procedia Eng.*, **2012**, *49*, 348-356.
- (a) Reece, S. Y.; Hamel, J. A.; Sung, K.; Jarvi, T. D.; Esswein, A. J.; Pijpers, J. J. H.; Nocera, D. G. Wireless Solar Water Splitting Using Silicon-Based Semiconductors and Earth-Abundant Catalysts. *Science*, **2011**, *334*, 645-648; (b) Nocera, D. G. Chemistry of Personalized Solar Energy. *Inorg. Chem.*, **2009**, *48*, 10001-10017.
- (a) Rutherford W. A.; Moore, T. A. Mimicking photosynthesis, but just the best bits. *Nature*, **2008**, *453*, 449; (b) Balzani, V.; Credi A.; Venturi, M. Photochemical Conversion of Solar Energy. *Chem. Sus. Chem.*, **2008**, *1*, 26-58; (c) Benniston, A. C.; Harriman, A. Artificial photosynthesis. *Mater. Today*, **2008**, *11*, 26-34; (d) Gray, H. B. Powering the planet with solar fuel. *Nature Chem.*, **2009**, *1*, 7; (e)

- Magnuson, A.; Anderlund, M.; Johansson, O.; Lindblad, P.; Lomoth, R.; Polivka, T.; Ott, S.; Stensjö, K.; Styring, S.; Sundström V.; Hammarström, L. Biomimetic and Microbial Approaches to Solar Fuel Generation. *Acc. Chem. Res.*, **2009**, *42*, 1899-1909; (f) Nocera, D. G. The Artificial Leaf. *Acc. Chem. Res.*, **2012**, *45*, 767-776; (g) Wasielewski, M. R. Energy, Charge, and Spin Transport in Molecules and Self-Assembled Nanostructures Inspired by Photosynthesis. *J. Org. Chem.*, **2006**, *71*, 5051-5066; (h) Bard A. J.; Fox, M. A. Artificial Photosynthesis: Solar Splitting of Water to Hydrogen and Oxygen. *Acc. Chem. Res.*, **1995**, *28*, 141-145; (i) M. Grätzel, Photoelectrochemical cells. *Nature*, **2001**, *414*, 338-344; (j) Hambourger, M.; Moore, G. F.; Kramer, D. M.; Gust, D.; Moore A. L.; Moore, T. A. Biology and technology for photochemical fuel production. *Chem. Soc. Rev.*, **2009**, *38*, 25-35; (k) Alstrum-Acevedo, J. H.; Brennaman M. K.; Meyer, T. J. Chemical Approaches to Artificial Photosynthesis. 2. *Inorg. Chem.*, **2005**, *44*, 6802-6827; (l) Knör, G. Recent progress in homogeneous multielectron transfer photocatalysis and artificial photosynthetic solar energy conversion. *Coord. Chem. Rev.*, **2015**, *304-305*, 102-108.
- 8 O'Regan, B.; Grätzel, M. A low-cost, high-efficiency solar cell based on dye-sensitized colloidal TiO₂ film. *Nature*, **1991**, *353*, 737-740.
- 9 (a) Boulas, P. L.; Gomez-Kaifer M.; Echegoyen, L. Electrochemistry of Supramolecular Systems. *Angew. Chem. Int. Ed.*, **1998**, *37*, 216-247; (b) Xie, Q.; Pérez-Cordero E.; Echegoyen, L. Electrochemical Detection of C₆₀⁶⁻ and C₇₀⁶⁻: Enhanced Stability of Fullerides in Solution. *J. Am. Chem. Soc.*, **1992**, *114*, 3978-3980. (c) Ruben, M.; Breuning, E.; Gisselbrecht J.-P.; Lehn, J.-M. Multilevel molecular electronic species: Electrochemical reduction of a [2 × 2] Co(II)₄ grid-type complex by 11 electrons in 10 reversible steps. *Angew. Chem. Int. Ed.*, **2000**, *39*, 4139-4142.
- 10 (a) Astruc, D. Ferrocenyl dendrimers: multi-electron redox reagents and their applications. *New J. Chem.*, **2011**, *35*, 764-772 and references therein; (b) Ronconi, C. M.; Stoddart, J. F.; Balzani, V.; Baroncini, M.; Ceroni, P.; Giansante C.; Venturi, M. Polyviologen Dendrimers as Hosts and Charge-Storing Devices. *Chem.-Eur. J.*, **2008**, *14*, 8365-8373; (c) Mayor, M.; Lehn, J.-M. Reducible Nanosize Macrocycles. *J. Am. Chem. Soc.* **1999**, *121*, 11231-11232.
- 11 For an example of a one-photon gated reversible C-C bond, see: Waidhas, F.; Jevric, M.; Fromm, L.; Bertram, M.; Görling, A.; Moth-Poulsen, K.; Brummel, O.; Libuda, J. Electrochemically controlled energy storage in a norbornadiene-based solar fuel with 99% reversibility. *Nano Energy* **2019**, *63*, 103872 and references therein.
- 12 Adams, D. M. et al. Charge Transfer on the Nanoscale: Current Status. *J. Phys. Chem. B*, **2003**, *107*, 6668-6697 and references therein.
- 13 (a) Kertesz, M. Pancake Bonding: An Unusual Pi-Stacking Interaction. *Chem. - Eur. J.*, **2019**, *25*, 400-416; (b) Mou Z.; Kertesz, M. Sigma-versus Pi-Dimerization Modes of Triangulene. *Chem. - Eur. J.*, **2018**, *24*, 6140-6147.
- 14 Fortage, J.; Peltier, C.; Nastasi, F.; Puntoriero, F.; Tuyères, F.; Griveau, S.; Bedioui, F.; Adamo, C.; Ciofini, I.; Campagna S.; Lainé, P. P. Designing Multifunctional Expanded Pyridiniums: Properties of Branched and Fused Head-to-Tail Bipyridiniums. *J. Am. Chem. Soc.*, **2010**, *132*, 16700-16713.
- 15 Marder, S. R.; Cheng, L.-T.; Tiemann, B. G.; Friedli, A. C.; Blanchard-Desce, M.; Perry J. W.; Skindhej, J. Large First Hyperpolarizabilities in Push-Pull Polyenes by Tuning of the Bond

- Length Alternation and Aromaticity. *Science*, **1994**, *263*, 511-514.
- 16 (a) Fortage, J.; Peltier, C.; Perruchot, C.; Takemoto, Y.; Teki, Y.; Bedioui, F.; Marvaud, V.; Dupeyre, G.; Pospíšil, L.; Adamo, C.; Hromadová, M.; Ciofini, I.; Lainé, P. P. Single-Step versus Stepwise Two-Electron Reduction of Polyarylpiperidiniums: Insights from the Steric Switching of Redox Potential Compression. *J. Am. Chem. Soc.*, **2012**, *134*, 2691-2705; (b) Lachmanová, Š.; Dupeyre, G.; Tarábek, J.; Ochsenbein, P.; Perruchot, C.; Ciofini, I.; Hromadová, M.; Pospíšil, L.; Lainé, P. P. Kinetics of Multielectron Transfers and Redox-Induced Structural Changes in N-Aryl-Expanded Piperidiniums: Establishing Their Unusual, Versatile Electrophoric Activity. *J. Am. Chem. Soc.*, **2015**, *137*, 11349-11364.
- 17 Pascal Jr., R. A. Twisted Acenes. *Chem. Rev.*, **2006**, *106*, 4809-4819.
- 18 Cross, W.; Hawkes, G. E.; Kroemer, R. T.; Liedl, K. R.; Loerting, T.; Nasser, R.; Pritchard, R. G.; Steele, M.; Watkinson, M.; Whiting, A. The structure, modelling and dynamics of hindered 5,6-diarylnaphthalenes. *J. Chem. Soc., Perkin Trans. 2*, **2001**, 459-467.
- 19 (a) Brown, H. C.; Bartholomay Jr. H.; Taylor, M. D. Acid-Base Studies in Gaseous Systems. 11. The Anomalous Base Strength of the Methylamines; A New Manifestation of Steric Strain. *J. Am. Chem. Soc.*, **1944**, *66*, 435-442; (b) Hounshell, W. D.; Dougherty, D. A.; Hummel, J. P.; Mislow, K. Structure of Hexaphenylethane and Congeners as Determined by Empirical Force Field Calculations. *J. Am. Chem. Soc.*, **1977**, *99*, 1916-1924.
- 20 (a) Lima, C. F. R. A. C.; Rocha, M. A. A.; Gomes, L. R.; Low, J. N.; Silva, A. M. S.; Santos, L. M. N. B. F. Experimental Support for the Role of Dispersion Forces in Aromatic Interactions. *Chem.-Eur. J.*, **2012**, *18*, 8934-8943; (b) Pieters, G.; Terrasson, V.; Gaucher, A.; Prim, D.; Marrot, J. Synthesis and Molecular Structure of Symmetrical 1,8-Diarylnaphthalenes. *Eur. J. Org. Chem.*, **2010**, *30*, 5800-5806.
- 21 (a) Bondi, A. van der Waals Volumes and Radii. *J. Phys. Chem.*, **1964**, *68*, 441-451; (b) Chebny, V. J.; Shukla, R.; Rathore, R. Toroidal Hopping of a Single Hole through the Circularly-Arrayed Naphthyl Groups in Hexanaphthylbenzene Cation Radical. *J. Phys. Chem. A*, **2006**, *110*, 13003-13006.
- 22 It's worth noting that the potentially repelling cationic charges are not located at the short contact site where bond formation is expected, hence reducing accordingly electrostatic strain (demand) within the native assembly.
- 23 When using the reading grid of electrochemical reactivity in the potential range spanning from -2V to +1V (vs. SCE in acetonitrile), the sole pyridinium groups, that are spatially disjointed, are redox active. They are structurally gathered by the electrochemically-inactive naphthalene scaffold, hence the notion of supramolecular assemblies used for these super-electrophores within the present context of electrochemistry. This reading grid is very similar to that perfected by V. Balzani²⁴ for the field of Supramolecular Photochemistry, in the context of photochemistry.
- 24 (a) Balzani, V.; Moggi, L.; Scandola, F. in *Supramolecular Photochemistry*, (Eds.: V. Balzani, D. Reidel) Publishing Co., Dordrecht, The Netherlands, **1987**, pp. 1-28; (b) Balzani, V. *Supramolecular Photochemistry*. *Tetrahedron*, **1992**, *48*, 10443-10514.
- 25 As regards MVs, it is worth noting that close cofacial contact of these electrophores is likely to impact their electronic structure and reactivity. This phenomenon is observed whether these MVs are tightly tethered, in high concentration, organized in self-assembled monolayers or encapsulated in supramolecular host-guest assemblies. The result is the formation of π complex dimers exhibiting redox behaviors distinguishable from that of isolated MV. For representative references, see (a) Burgess, M.; Chénard, E.; Hernández-Burgos, K.; Nagarjuna, G.; Assary, R. S.; Hui, J.; Moore,

- 1
2
3 J. S.; Rodríguez-López, J. Impact of Backbone Tether Length and
4 Structure on the Electrochemical Performance of Viologen Redox
5 Active Polymers. *Chem. Mater.*, **2016**, *28*, 7362-7374; (b) MacInnes, M.
6 M.; Cousineau, B. R.; Youngs, S. M.; Sinniah, K.; Reczek, J. J.;
7 Maldonado, S. Discovery of Unusually Stable Reduced Viologen via
8 Synergistic Folding and Encapsulation. *J. Electrochem. Soc.*, **2019**,
9 *166*, H825-H834; (c) Tang, X.; Schneider, T. W.; Walker, J. W.;
10 Buttry, D. A. Dimerized π -Complexes in Self-Assembled Monolayers
11 Containing Viologens: An Origin of Unusual Wave Shapes in the
12 Voltammetry of Monolayers. *Langmuir*, **1996**, *12*, 5921-5933.
- 13 26 Kanato, H.; Takimiya, K.; Otsubo, T.; Aso, Y.; Nakamura, T.; Araki
14 Y.; Ito, O. Synthesis and Photophysical Properties of Ferrocene-
15 Oligothiophene-Fullerene Triads. *J. Org. Chem.*, **2004**, *69*, 7183-7189.
- 16 27 Fortage, J.; Tuyèras, F.; Ochsenbein, P.; Puntoriero, F.; Nastasi,
17 F.; Campagna, S.; Griveau, S.; Bedioui, F.; Ciofini I.; Lainé, P. P.
18 Expanded Pyridiniums: Bis-cyclization of Branched Pyridiniums into
19 Their Fused Polycyclic and Positively Charged Derivatives—Assessing
20 the Impact of Pericondensation on Structural, Electrochemical,
21 Electronic, and Photophysical Features. *Chem. - Eur. J.*, **2010**, *16*,
22 11047-11063.
- 23 28 Clough, R. L.; Kung, W. J.; Marsh R. E.; Roberts, J. D. Structural
24 Analysis of Internally Crowded Naphthalene Derivatives. peri-
25 Diphenylacenaphthene. *J. Org. Chem.*, **1976**, *41*, 3603-3609.
- 26 29 Schmidt, H. C.; Spulber, M.; Neuburger, M.; Palivan, C. G.; Meuwly
27 M.; Wenger, O. S. Charge Transfer Pathways in Three Isomers of
28 Naphthalene-Bridged Organic Mixed Valence Compounds. *J. Org. Chem.*,
29 **2016**, *81*, 595-602; and references cited therein.
- 30 30 (a) Connelly N. G.; Geiger, W. E. Chemical Redox Agents for
31 Organometallic Chemistry. *Chem. Rev.*, **1996**, *96*, 877-910; (b) Balej,
32 J. Standard potential of sodium amalgam at 25°C. *Electrochim. Acta*,
33 **1976**, *21*, 953-956.
- 34 31 Noteworthy, calculated chemical shifts using DFT were in good
35 agreement with the experiments and gives some insight on the nature
36 of 2^0 (see Section S11 in SI). An important geometry change was
37 calculated from the native form $2[PF_6]_2$ to the reduced form 2^0 in
38 agreement with the loss of aromaticity and the emergence of a
39 quinoid form for the pyridinium subunits.
- 40 32 Evans, D. H. One-Electron and Two-Electron Transfers in
41 Electrochemistry and Homogeneous Solution Reactions. *Chem. Rev.*,
42 **2008**, *108*, 2113-2144 and references therein.
- 43 33 There is no specific reference but one can take the instance of bond
44 formation in dihydrogen molecule: Caruso, F.; Rohr, D. R.; Hellgren,
45 M.; Ren, X.; Rinke, P.; Rubio A.; Scheffler, M. Bond Breaking and
46 Bond Formation: How Electron Correlation is Captured in Many-Body
47 Perturbation Theory and Density-Functional Theory. *Phys. Rev. Lett.*,
48 **2013**, *110*, 146403.
- 49 34 For the Red-1 process of 2^{2+} , the measurement of $|E_p - E_{p/2}|$ (where $E_{p/2}$
50 is the half-peak potential) was found to be 38 mV, which agrees with
51 a bi-electronic process for an irreversible system.³⁵ As regards 1^+ ,
52 the $|E_p - E_{p/2}|$ value of the Red-1 process amounts to 51.6 mV, as
53 approximately expected for a reversible mono-electronic process.³⁴
- 54 35 Bard, A. J.; Faulkner, L. R. *Electrochemical Methods. Fundamentals*
55 *and Applications*, Second Ed., Chapter 6, Wiley, New York, **2001**.
- 56 36 $E_{1/2}$ is calculated as $(E_{pa} + E_{pc})/2$, where E_{pa} and E_{pc} are the anodic and
57 cathodic peak potentials.
- 58 37 Electrophoric concentrations used for electrochemical studies
59 reported in ref. 16a were about 0.5 mM, like here, instead of 5 mM,
60 as incorrectly indicated in the experimental section of this paper.
- 38 Given that the current varies as the square root of the potential
scan rate ($v^{1/2}$), direct comparison of CVs recorded at different scan

1
2
3 rates (0.1 V s^{-1} and 0.625 V s^{-1}) is therefore possible provided that
4 actual current is normalized against $v^{1/2}$. This data treatment also
5 justifies the choice of peculiar v values (e.g. 25, 100, 225, 400 or
6 625 mV s^{-1}) in electrochemical studies where the impact of the rate
7 of applied voltage is investigated (e.g. Current I (mA) as the
8 function of $v^{1/2}$ (v in mV s^{-1})), as it gives convenient incremental $v^{1/2}$
9 values (i.e. 5, 10, 15, 20 or 25 $\text{mV}^{1/2} \text{ s}^{-1/2}$); see Figure S17 in SI.

10
11 39 By plotting (I_{red}/v) versus ($v^{1/2}$) (see Figure S17 in Section S25.2 of
12 the SI), where I_{red} is the cathodic peak current, a linear
13 relationship is obtained for both mono- and di-pyridinium assemblies
14 (**1** and **2**). This observation clearly demonstrates that (1) there is
15 no adsorption of the electroactive species at the Pt electrode
16 surface and (2) the current is controlled by a semi-infinite linear
diffusion process.

17
18 40 Home-made codes were written for the convolution analysis using
19 algorithm suggested by Oldham; see Oldham, K. B. Convolution: A
20 General Electrochemical Procedure Implemented by a Universal
Algorithm, *Anal. Chem.*, **1986**, 582, 2296-2300.

21
22 41 Teplý, F.; Čížková, M.; Slavíček, P.; Kolivoška, V.; Tarábek, J.;
23 Hromadová M.; Pospíšil, L. Electron Transfer Triggers Fast
24 Dimer/Monomer Switching of Pyridinium and Quinolinium Cations. *J.*
Phys. Chem. C, **2012**, 116, 3779-3786.

25
26 42 Hromadová, M.; Pospíšil, L.; Sokolová R.; Kolivoška, V.
27 Electrochemical reduction of dodecylpyridinium bromide in aprotic
28 solvents: mechanistic studies. *Collect. Czech. Chem. Commun.*, **2011**,
29 76, 1895-1908.

30
31 43 Brandt, J. R.; Pospíšil, L.; Bednářová, L.; Correa da Costa, R.;
32 White, A. J. P.; Mori, T.; Teplý F.; Fuchter, M. J. Intense redox-
33 driven chiroptical switching with a 580 mV hysteresis actuated
34 through reversible dimerization of an azoniahelicene. *Chem. Commun.*,
35 **2017**, 53, 9059-9062.

36
37 44 Plutnar, J.; Hromadová, M.; Ramešová, Š.; Havlas Z.; Pospíšil, L.
38 Electron Transfer Mechanism of Substituted Benzimidazoles: Dimer
39 Switching, Oscillations, and Search for Singlet Fission Properties.
40 *J. Phys. Chem. C.*, **2017**, 121, 9963-9969.

41
42 45 Mairanovsky, S. G. The polarographic behavior of quaternary
43 pyridinium salts. *Dokl. Akad. Nauk SSSR*, **1956**, 110, 593-596.

44
45 46 (a) Michaelis, L.; Hill, E. S. The viologen indicators. *J. Gen.*
46 *Physiol.*, **1933**, 16, 859-873; (b) Dimroth O.; Hoene, R. Reduction of
47 pyridine with zinc dust and acetic acid anhydride. *Ber. Dtsch. Chem.*
48 *Ges.*, **1921**, 54, 2934-2942.

49
50 47 Koutecký, J.; Hanuš, V. Zwei Beispiele schneller, in den
51 Depolarisationvorgang an der Tropfenelektrode eingeschalteter,
52 bimolekularer Reaktionen. *Collect. Czech. Chem. Commun.*, **1955**, 20,
53 124-138.

54
55 48 Gaudiello, J. G.; Larkin, D.; Rawn, J. D.; Bancroft E. E.; Blount,
56 H. N. On the mechanism of the electrochemical reduction of *N*-
57 methylpyridinium ion. *J. Electroanal. Chem.*, **1982**, 131, 203-214.

58
59 49 Olmstead, M. L.; Hamilton R. G.; Nicholson, R. S. Theory of Cyclic
60 Voltammetry for a Dimerization Reaction Initiated Electrochemically.
Anal. Chem., **1969**, 41, 260-267.

61
62 50 Andrieux, C. P.; Nadjó L.; Savéant, J.-M. Electrodimerization: I.
63 One-electron irreversible dimerization. Diagnostic criteria and rate
64 determination procedures for voltammetric studies. *J. Electroanal.*
65 *Chem.*, **1970**, 26, 147-186.

66
67 51 (a) Imbeaux J. C.; Savéant, J.-M. Convulsive potential sweep
68 voltammetry: I. Introduction. *J. Electroanal. Chem.*, **1973**, 44, 169-
69 187; (b) Ammar, F.; Savéant, J.-M. Convulsive potential sweep
70 voltammetry: II. Multistep Nernstian waves. *J. Electroanal. Chem.*,
1973, 47, 215-221.

- 1
2
3 52 Hall, G. B.; Kottani, R.; Felton, G. A. N.; Yamamoto, T.; Evans, D.
4 H.; Glass R. S.; Lichtenberger, D. L. Intramolecular Electron
5 Transfer in Bipyridinium Disulfides. *J. Am. Chem. Soc.*, **2014**, *136*,
6 4012-4018.
- 7 53 Suzuki, T.; Nishida J.-i.; Tsuji, T. A new type of tricolor
8 electrochromic system based on the dynamic redox properties of
9 hexaarylethane derivatives. *Chem. Commun.*, **1998**, 2193-2194.
- 10 54 Suzuki, T.; Takeda, T.; Kawai H.; Fujiwara, K. Ultralong C-C bonds
11 in hexaphenylethane Derivatives. *Pure Appl. Chem.*, **2008**, *80*, 547-
12 553.
- 13 55 Suzuki, T.; Takeda, T.; Ohta, E.; Wada, K.; Katoono, R.; Kawai H.;
14 Fujiwara, K. Bis(10-methylacridinium)s as a Versatile Platform for
15 Redox-Active Functionalized Dyes and Novel Structures. *Chem. Rec.*,
16 **2015**, *15*, 280-294.
- 17 56 Takeda, T.; Uchimura, Y.; Kawai, H.; Katoono, R.; Fujiwara K.;
18 Suzuki, T. Hexaphenylethanes with an Ultralong CC Bond:
19 Expandability of the CC Bond in Highly Strained Tetraarylpyracenes.
20 *Chem. Lett.*, **2013**, *42*, 954-962.
- 21 57 Bettinger, H. F.; Schleyer P. v. R.; Schaefer III, H. F.
22 Tetraphenyldihydrocyclobutanes – what causes the extremely long
23 1.72 Å C-C single bond?. *Chem. Commun.*, **1998**, 769-770.
- 24 58 Kammermeier, S.; Jones P. G.; Herges, R. [2 + 2] Cycloaddition
25 Products of Tetradehydroanthracene : Experimental and Theoretical
26 Proof of Extraordinary Long C - C Single Bonds. *Angew. Chem., Int.*
27 *Ed. Engl.*, **1997**, *36*, 1757-1760.
- 28 59 Pauling, L. *The Nature of the Chemical Bond and the Structure of*
29 *Molecules and Crystals*, 3rd ed.; Cornell University Press: Ithaca,
30 NY, **1960**; Chapters 7 and 8.
- 31 60 Zavitsas, A. A. The Relation between Bond Lengths and Dissociation
32 Energies of Carbon-Carbon Bonds. *J. Phys. Chem. A*, **2003**, *107*, 897-
33 898.
- 34 61 Suzuki, T. Nishida J.-I.; Tsuji, T. Hexaphenylethane Derivatives
35 Exhibiting Novel Electrochromic Behavior. *Angew. Chem., Int. Ed.*
36 *Engl.*, **1997**, *36*, 1329-1331.
- 37 62 (a) Horner M.; Hünig. S. Conjugation in Bicyclo[1.1.0]butanes. LUMO
38 Properties of the Bridging Bond. *J. Am. Chem. Soc.*, **1977**, *99*, 6122-
39 6124; (b) Hünig, S.; Briehn, C. A.; Bäuerle P.; Emge, A.
40 Electrochromics by Intramolecular Redox Switching of Single Bonds.
41 *Chem.-Eur. J.*, **2001**, *7*, 2745-2757.
- 42 63 For an example of electrochemically gated covalent sulfur-sulfur
43 bond formation/cleavage, see refs 52 and Benniston, A. C.; Hagon,
44 J.; He, X.; Yang S.; Harrington, R. W. Spring Open Two-plus-Two
45 Electron Storage in a Disulfide-Strapped Methyl Viologen Derivative.
46 *Org. Lett.*, **2012**, *14*, 506-509.
- 47 64 (a) Suzuki, T.; Wada, K.; Ishigaki, Y.; Yoshimoto, Y.; Ohta, E.;
48 Kawai H.; Fujiwara, K. Drastic change in racemization barrier upon
49 redox reactions: novel chiral-memory units based on dynamic redox
50 systems. *Chem. Commun.*, **2010**, *46*, 4100-4102; (b) Suzuki, T.;
51 Ishigaki, Y.; Iwai, T.; Kawai, H.; Fujiwara, K.; Ikeda, H.; Kano Y.;
52 Mizuno, K. Multi-Input/Multi-Output Molecular Response System Based
53 on the Dynamic Redox Behavior of 3,3,4,4 Tetraaryldihydro[5]helicene
54 Derivatives: Reversible Formation/Destruction of Chiral Fluorophore
55 and Modulation of Chiroptical Properties by Solvent Polarity. *Chem.*
56 *Eur. J.*, **2009**, *15*, 9434-9441; (c) Suzuki, T.; Sakano, Y.; Iwai, T.;
57 Iwashita, S.; Miura, Y.; Katoono, R.; Kawai, H.; Fujiwara, K.; Tsuji
58 Y.; Fukushima, T. 7,7,8,8-Tetraaryl-o-quinodimethane Stabilized by
59 Dibenzo Annulation: A Helical π -Electron System That Exhibits
60 Electrochromic and Unique Chiroptical Properties. *Chem. -Eur. J.*,
2013, *19*, 117-123.
- 61 (a) Ohta, E.; Nehira, T.; Kawai, H.; Fujiwara K.; Suzuki, T. Four-
62 way-output molecular response system based on the

- 1
2
3 dihydrodibenzo[c,g]phenanthrene skeleton: modulation of CD and FDCD
4 activity by acid and electron-transfer. *Tetrahedron Lett.*, **2008**, *49*,
5 777-781; (b) Nishida, J.-I.; Miyagawa T.; Yamashita, Y. Novel
6 Thiophene Oligomers Containing a Redox Active Hexaarylethane Unit.
7 *Org. Lett.*, **2004**, *6*, 2523-2526.
- 8 66 Suzuki, T.; Tanaka, S.; Kawai H.; Fujiwara, K. Multi-input-Multi-
9 output Molecular Response System Based on Dynamic Redox Behavior of
10 Hexaphenylethane-type Electron Donors with the
11 Tetrahydrophenanthrazepine Skeleton: Strong Chiroptical Signals
12 through the Transmission of Point Chirality to Helicity. *Chem. Asian*
13 *J.*, **2007**, *2*, 171-177.
- 14 67 (a) Logtenberg H.; Browne, W. R. Electrochemistry of
15 dithienylethenes and their application in electropolymer modified
16 photo- and redox switchable surfaces. *Org. Biomol. Chem.*, **2013**, *11*,
17 233-243; (b) Staykov, A.; Areephong, J.; Browne, W. R.; Feringa B.
18 L.; Yoshizawa, K. Electrochemical and Photochemical Cyclization and
19 Cycloreversion of Diarylethenes and Diarylethene-Capped
20 Sexithiophene Wires. *ACS Nano*, **2011**, *5*, 1165-1178; (c) Gilat, S. L.;
21 Kawai S. H.; Lehn, J.-M. Light-Triggered Molecular Devices:
22 Photochemical Switching of Optical and Electrochemical Properties in
23 Molecular Wire Type Diarylethene Species. *Chem. -Eur. J.*, **1995**, *1*,
24 275-284; (d) Peters A.; Branda, N. R. Electrochemically induced
25 ring-closing of photochromic 1,2-dithienylcyclopentenes. *Chem.*
26 *Commun.*, **2003**, 954-955; (e) Gorodetsky, B.; Samachetty, H. D.;
27 Donkers, R. L.; Workentin M. S.; Branda, N. R. Reductive
28 Electrochemical Cyclization of a Photochromic 1,2-
29 Dithienylcyclopentene Dication. *Angew. Chem., Int. Ed. Engl.*, **2004**,
30 *43*, 2812-2815; (f) Moriyama, Y.; Matsuda, K.; Tanifuji, N.; Irie S.;
31 Irie, Electrochemical Cyclization/Cycloreversion Reactions of
32 Diarylethenes. *Org. Lett.*, **2005**, *7*, 3315-3318.
- 33 68 Rathore, R.; Le Magueres, P.; Lindeman S. V.; Kochi, J. K. A Redox-
34 Controlled Molecular Switch Based on the Reversible C-C Bond
35 Formation in Octamethoxytetraphenylene. *Angew. Chem. Int. Ed.* **2000**,
36 *39*, 809-812.
- 37 69 (a) Kawai, H.; Takeda, T.; Fujiwara, K.; Wakeshima, M.; Hinatsu Y.;
38 Suzuki, T. Ultralong Carbon-Carbon Bonds in Dispirobis(10-
39 methylacridan) Derivatives with an Acenaphthene, Pyracene, or
40 Dihydropyracylene Skeleton. *Chem. Eur. J.*, **2008**, *14*, 5780-5793; (b)
41 Suzuki, T.; Yoshimoto, Y.; Takeda, T.; Kawai H.; Fujiwara, K.
42 Intramolecular Methylacridan-Methylacridinium Complexes with a
43 Phenanthrene-4,5-diyl or Related Skeleton: Geometry-Property
44 Relationships in Isolable C-H Bridged Carbocations. *Chem. - Eur. J.*,
45 **2009**, *15*, 2210-2216; (c) Wada, K.; Takeda, T.; Kawai, H.; Katoono,
46 R.; Fujiwara K.; Suzuki, T. Geometrical Remote Steric Effects in
47 4,5-Disubstituted-9,10-dihydrophenanthrenes: Expansion of
48 Prestrained C⁹-C¹⁰ Bond in Di(spiroacridan) Derivatives. *Chem. Lett.*,
49 **2013**, *42*, 1194-1196; (d) Suzuki, T.; Migita, A.; Higuchi, H.; Kawai,
50 H.; Fujiwara K.; Tsuji, T. A novel redox switch for fluorescence:
51 drastic UV-vis and fluorescence spectral changes upon electrolysis
52 of a hexaphenylethane derivative of 10,10'-dimethylbiacridan.
53 *Tetrahedron Lett.*, **2003**, *44*, 6837-6840; (e) Kawai, H.; Takeda, T.;
54 Fujiwara K.; Suzuki, T. Short nonbond and long C-C bond in
55 naphthalene-1,8-diylbis(10-methylacridinium) and the corresponding
56 hexaphenylethane derivative: a new electrochromic pair exhibiting
57 dynamic redox properties. *Tetrahedron Lett.*, **2004**, *45*, 8289-8293;
58 (f) Suzuki, T.; Ohta, K.; Nehira, T.; Higuchi, H.; Ohta, E.; Kawai
59 H.; Fujiwara, K. Unprecedented four-way-output molecular response
60 system based on biphenyl-2,20-diylldiacridiniums: induction of axial
chirality through intramolecular hydrogen bonds between chiral amide
groups. *Tetrahedron Lett.*, **2008**, *49*, 772-776.

- 1
2
3
4
5
6
7
8
9
10
11
12
13
14
15
16
17
18
19
20
21
22
23
24
25
26
27
28
29
30
31
32
33
34
35
36
37
38
39
40
41
42
43
44
45
46
47
48
49
50
51
52
53
54
55
56
57
58
59
60
- 70 Luisi, P. L. Emergence in Chemistry: Chemistry as the Embodiment of
Emergence. *Foundat. Chem.*, **2002**, *4*, 183-200.
- 71 Of note, there exists a category of organic molecules denoted "Super
Electron Donors", SED, that stores couples of electrons in chemical
bonds and can serve as powerful reducers ("organic sodium"). Their
limitation stems in the fact that they can be used only once
(discharging); see for instance refs. (a) Murphy, J. A. Discovery
and Development of Organic Super-Electron-Donors. *J. Org. Chem.*
2014, *79*, 3731-3746; (b) Doni E.; Murphy, J. A. Evolution of neutral
organic super-electron donors and their applications. *Chem. Commun.*,
2014, *50*, 6073-6087; (c) Zhou, S.; Anderson, G. M.; Mondal, B.;
Doni, E.; Ironmonger, V.; Kranz, M.; Tuttle T.; Murphy, J. A.
Organic super-electron-donors: initiators in transition metal-free
haloarene-arene coupling. *Chem. Sci.*, **2014**, *5*, 476-482.
- 72 Muench, S.; Wild, A.; Friebe, C.; Häupler, B.; Janoschka T.;
Schubert, U. S. Polymer-Based Organic Batteries. *Chem. Rev.*, **2016**,
116, 9438-9484.
- 73 Antoni, P. W.; Bruckhoff T.; Hansmann, M. M. Organic Redox Systems
Based on Pyridinium-Carbene Hybrids. *J. Am. Chem. Soc.*, **2019**, *141*,
9701-9711.
- 74 Nomrowski J.; Wenger, O. S. Exploiting Potential Inversion for
Photoinduced Multielectron Transfer and Accumulation of Redox
Equivalents in a Molecular Heptad. *J. Am. Chem. Soc.*, **2018**, *140*,
5343-5346.

TOC Graphic

